OXIDATIVE COUPLING OF METHANE OVER LITHIUM DOPED MAGNESIUM OXIDE

by

Manouchehr Nadjafi

B.S., Chemical Engineering, Sahand University of Technology, 2010

Submitted to the Institute for Graduate Studies in
Science and Engineering in partial fulfillment of
the requirements for the degree of
Master of Science

Graduate Program in Chemical Engineering
Boğaziçi University

2015

OXIDATIVE COUPLING OF METHANE OVER LITHIUM DOPED MAGNESIUM OXIDE

APPROVED BY:

Prof. Ramazan Yıldırım (Thesis Supervisor)	……..
Assoc. Prof. Ahmet Kerim Avcı	……..
Assist. Prof. Mehmet Erdem Günay	……..

DATE OF APPROVAL:

to my Cıkıs

ACKNOWLEDGEMENTS

First and most, I would like to express my sincerest gratitude to my supervisor, Dr. Ramazan Yıldırım, who has supported me throughout my thesis with his endless patience and knowledge whilst allowing me the room to work in my own way. He brings me different perspective during my research and keeps my interest and excitement on the project. This dissertation would not have been possible without his inspiration and effort.

I would like to express my very sincere gratitude to Dr. Mehmet Erdem Günay for his detailed comments on my thesis and special thanks to Dr. Ahmet Kerim Avcı for valuable discussion during my thesis defense. Both of them gave me valuable suggestions. I also want to express my great appreciation for Dr. Zeynep İlsen Önsan for her sincere support and encouragement during my master degree in Turkey. I always was inspired by her knowledge and motivation. I am thankful to Dr. Kerem Uğuz for his encouragements and inspirations.

Very special thanks to A. Neslihan Şener, Melek Selcen Başar, and Elif Erdinç for their friendship, endless support and their valuable help and comments on my thesis abstract and presentation. I am also very thankful to my family for their patience and support during my Master degree in Turkey.

I would like to thank C. Doğa Demirhan, Barış Burnak, Elif Can, Elif Gençtürk, Emre Demirel, Mohammad Beygi, Mehran Torabi, Yeşim Düşova, Özgü Özer, Özgür Y. Çağlar, Aybüke Leba, A. İpek Paksoy, Merve Eropak, Ali Uzun, Serhat Erşahin, B. Kerem Aksakal, Çağla Odabaşı, Onur Kavaklı, Sinan Koç, and all CATREL team. It was my pleasure to be part of such a great team.

Special thanks to Murat Düzgünoğlu, Bilgi Dedeoğlu, Yakup Bal, Belgin Balkan, Melike Gürbüz, and Esma Toprak for their technical aid as well as their heartfelt friendship.

The financial support for this thesis, provided by TÜBİTAK through project 112M714 is gratefully acknowledged.

ABSTRACT

OXIDATIVE COUPLING OF METHANE OVER LITHIUM DOPED MAGNESIUM OXIDE

In this study, a monolithic structure was employed for oxidative coupling of methane reaction over lithium doped magnesium oxide catalyst and the results were compared to those over the particulate catalyst. The rationale behind the study was to see the effects of empty space within the monolith on C_2 (C_2H_4 and C_2H_6) yield; and effects of monolithic structure on the stability of Li/MgO catalyst at harsh conditions of OCM reaction. 0.5 wt.% Li/MgO particulate catalyst was prepared by wet impregnation and mixed mill technique while the monolith catalyst was prepared by dip-coating technique. Furthermore, two different precursors of lithium ($LiNO_3$ and CH_3COOLi) in the particulate catalyst preparation were also investigated. All the tests were carried out in a 10 mm internal diameter quartz reactor, which had a reduced part (2 mm) exactly after the catalyst bed in order to evacuate produced gases immediately from the reaction medium. This was done to minimize gas phase reactions and send product gases to the condensers. SEM, EDX, and XRD tests were also done on the catalysts to see morphological and quantitative changes in the Li/MgO catalysts before and after catalytic tests. SEM images illustrate loss of Li during the reaction; considering this drawback, time on stream tests were done to see activity and selectivity changes by time. Experiments showed a drastic activity and selectivity decrease for particulate catalyst within first two hours of reactant gases introduction, which continued for the next hours in lesser extent. On the other hand, monolithic structure showed a poor activity and selectivity in comparison with particulate catalyst even though the stability seem to be increased by the use of monolithic structure. It is believed that poor performance of monolithic structure is related to its poor heat transfer. Reinforced monolith with metal framework, which is heated using an induction furnace is proposed as a promising technology for further investigations.

ÖZET

Li/MgO KATALİZÖRÜ ÜZERİNDE METANIN OKSİJEN VARLIĞINDA YÜKSEK HİDROKARBONLU MOLEKÜLLERE DÖNÜŞÜMÜ

Bu çalışmada, metanın oksijen varlığında yüksek hidrokarbonlu moleküllere dönüşümü hem monolitik yapıda hem de toz halde 0.5 wt.% Li/MgO katalizörü üzerinde incelenmiştir. Çalışma, temel olarak, hem monolit içersindeki boşluğun C_2 (C_2H_4 + C_2H_6) verimine hem de mullite yapının zorlu OCM reaksiyonu şartlarında Li/MgO katalizörünün kararlığına etkilerini görmeyi amaçlamıştır. Li/MgO katalizörünün hazirlanmasinda, toz halinde ıslak emdirme ve karışık öğütme, monolit halinde ise batırarak-kaplama teknikleri kullanılmıştır. Toz katalizörün hazırlanmasında lityumun iki farklı öncül maddesi ($LiNO_3$ and CH_3COOLi) incelenmiştir. Tüm testler iç çapı 10 mm olan ve üretilen gazların hemen tahliye edilebilmesi için katalizör yatağından sonra çapı 2 mm ye düşürülen kuvars reaktörde gerçekleştirilmiştir. Bu işlem gaz fazı reaksiyonlarının en aza indirgenmesi ve üretilen gazların yoğuşturucuya gönderilebilmesi için yapılmıştır. Li/MgO katalizörünün morfolojik yapısını ve reaksiyon sırasındaki katalizördeki kütle değişimini analiz etmek için katalitik testlerden önce ve sonra SEM, EDX ve XRD testleri yapılmıştır. SEM görüntüsü reaksiyon sırasındaki lityum kaybını göstermektedir. Reaksiyon sırasındaki lityum kaybının etkilerini görebilmek için aktivite testlerini tek bir reaktörde kalış süresinde (time on stream) değil farklı kalış sürelerinde yapılmıştır. Sonuçlar toz katalizörde aktivite ve seçicilik değerlerinin beslenen gazların sisteme gönderilmesinden sonraki ilk iki saat içinde çok düştüğünü ve ilerleyen saatlerde de ise bu düşüşün azalarak ta olsa devam ettiğini göstermektedir. Ayrıca monolitik yapının toz katalizörden, daha kararlı olmakla beraber (zaman içinde aktivite kaybı daha az), daha düşük aktivite ve seçicilik gösterdiği belirlenmiştir. Monolitik yapının ısı transferinin düşük olması sebebiyle performansının da zayıf olduğu düşünülmektedir. Güçlendirilmiş monolit ve içindeki metal yapının indüksiyonlu fırın ile ısıtılması ileride yapılacak araştırmalar için umut vaat eden bir çözüm olarak önerilmektedir.

TABLE OF CONTENTS

LIST OF FIGURES

LIST OF TABLES

LIST OF SYMBOLS

F	Flow rate
i	Gas i
I	Current
R	Resistance
X	Composition of gas

LIST OF ACRONYMS/ABBREVIATIONS

AAS	Atomic Absorption Spectroscopy
BET	Brunauer, Emmet, and Teller
CVD	Chemical Vapor Deposition
EDX	Energy Dispersive X-Ray
EPR	Electron Paramagnetic Resonance
FID	Flame Ionization detector
FSP	Flame Spray Technology
GC	Gas Chromatography
GHSV	Gas Hour Space Velocity
MFC	Mass Flow Controller
MIEMR	Mixed Ionic and Electronic Conducting Membrane Reactor
NMR	Nuclear Magnetic Resonance
OCM	Oxidative Coupling of Methane
PMR	Porous Membrane Reactor
SEM	Scanning Electron Microscopy
SOFCR	Solid Oxide Fuel Cell Reactor
STY	Space Time Yield
TCD	Thermal Conductivity Detector
TEM	Transmission Electron Microscopy
XPS	X-Ray Photoelectron Spectroscopy
XRD	X-Ray Powder Diffraction

1. INTRODUCTION

As the simplest hydrocarbon and main component of natural gas, methane can be obtained either from natural gas reservoirs or organic wastes as a component of biogas. Currently methane mainly used for energy production via combustion processes; only a small portion of methane is used for other purposes because it poses highest C-H bond energy among the alkanes [1]. Every year, a big portion of natural gas is flared into the atmosphere; it is 150×10^9 cubic meters, which is almost five percent of world total production at the end of 2011. World proved natural gas reserves at the end of 2014 stood at 187.1 trillion cubic meters (tcm), sufficient to meet 54.1 years of global production. Proved reserves grew by 0.3 % relative to end of 2013 while global consumption rate increased by 0.4% [2]. Depleting natural gas reserves, prompts us to use this valuable product in a more reasonable way.

One of the most challenging routs for methane utilization is oxidative coupling of methane (OCM) to ethane and ethylene. Ethylene and ethane are produced in situ while other sequential reactions may produce small amount of heavier hydrocarbons. Hydrocarbon products of OCM (ethane, ethylene, and higher hydrocarbons) often are reported as C_{2+} products. OCM target product is ethylene, not only because of its price but also because of market demand [3].

Ethylene is the raw material used in the production of important polymers such as polyethylene (PE), polyethylene terephthalate (PET), polyvinyl chloride (PVC), and polyester (PS) as well as fibers and other organic chemicals. These products are used in a wide variety of industrial and consumer markets such as packaging, transportation, electrical/electronic, textile and construction industries as well as consumer chemicals, coating and adhesives. Since the ethane can be also converted to ethylene, success in OCM process is very important for industry. However, beside these two desired reactions, undesired oxidation of the hydrocarbons (including C_2 products) to CO_x also takes place. There is a unanimous opinion that the initial step of the reaction is the formation of methyl radicals, which have been proven to exist [4, 5]. Once the formation of the radicals is initiated on a catalytic surface, gas-phase reactions are believed to proceed to a large extent. The

radicals should recombine selectively to ethane, which is then dehydrogenated to ethylene oxidatively or possibly also thermally. Meanwhile methoxy species formed on the surface or in the gas phase finally react to carbon dioxide [6].

In the hope of finding better catalyst for OCM, hundreds of materials have been tested. Among them Li/MgO catalyst showed supreme performance. Extensive research have been done on this catalyst and lots of details were published in the literature [7]. Nevertheless, this catalyst suffers from stability problem which is ignored in many studies. The objective of this study is to investigate stability of this catalyst on a mullite monolith.

Main purpose of this study was to investigate the effects of mullite monolith on yield and stability improvement of 0.5 wt.% Li/MgO catalyst for OCM reaction. For this reason, particulate catalyst tests were also done at the same conditions for comparison. In addition to the above mentioned comparison, two different precursor of Li ($LiNO_3$ and CH_3COOLi) prepared with mixed mill and wet impregnation method were also evaluated. Furthermore, best operational condition consisting of temperature, CH_4/O_2 ratio, and preparation method were investigated. EDX, SEM, and XRD results were used to support discussions and conclusions claimed here.

Chapter two starts with a brief introduction on OCM reaction and applied methods and catalysts. Main objective of this part is to focus on Li/MgO catalyst instead of general overview. For this purpose, Li/MgO catalyst preparation techniques are reviewed as a crucial factor in the performance and stability of this catalyst. Chapter two is continued with evaluation of performance and stability of this catalyst as well as the engineering aspects of process. Effect of additives, OCM mechanism over Li/MgO catalyst and monolith catalyst are discussed in the final sections of this Chapter. Chapter three provides an overview of chemicals, gases and apparatuses which are used in this study and explains details of experimental setup, operational conditions, and preparation techniques. Results are provided and discussed in Chapter 4 of this study which includes catalytic result of monolith and particulate catalyst and their morphological studies using SEM, EDX, and XRD. There are conclusion and recommendation Chapters numbered with 5 and 6 respectively which includes innovative solutions for problems addressed here.

2. LITERATURE SURVEY

The main constituent of natural gas (almost 85 %) is methane. Methane is a very stable, symmetrical molecule. Methane has a melting point of -182.5 ˚C and a boiling point of -161.5 ˚C. The C-H bonds are strong (425 kJ mol^{-1}) and it contains no functional group, magnetic moment or polar distribution to facilitate chemical attacks. Activation of methane by splitting of the C-H bond will require high temperatures and/or the use of oxidation agents. Catalysis will have to play an important role in most processes for methane conversion. Certain chemicals such as methanol are indirectly derived from methane through a reforming reaction, in which methane reacts with water at elevated temperatures to form hydrogen and carbon monoxide. Because of the enormous proven reserves of natural gas in the world, there is a strong economic incentive to develop a process that would convert methane into more valuable chemicals and fuels. The quest for such a process and the associated scientific challenge has stimulated a large amount of research over the last decade on methods for the direct conversion of methane into ethylene, methanol, formaldehyde, etc.[3]. However, despite a large research effort on the direct conversion of methane during the previous years, no breakthrough processes have been developed. The problems associated with the direct conversion of methane arise from both kinetics and thermodynamics. High temperatures are required for activation of methane and at such conditions radical reactions in the gas phase are dominating. The strength of the C-H bond in methane is stronger than in the possible products, meaning that the products will be more reactive than methane (the C-H bond strength in methanol is 389 kJ mol^{-1}). It means that the challenge in methane conversion is related to selectivity rather than reactivity. In order to circumvent these problems several different approaches based on catalysis and reaction engineering have been proposed and tested. In the following points, some of these approaches are described:

(i) Thermal and catalytic pyrolysis of methane.
(ii) Oxidative coupling of methane.
(iii) Partial oxidation of methane to methanol and formaldehyde.
(iv) Different processes (plasma, halogenation, photo-catalysis, membranes, etc.).

The number of possible products from the conversion of methane is limited to a few components such as C_2 hydrocarbons, benzene (aromatics), methanol, formaldehyde and carbon in addition to synthesis gas [5]. Chlorination to produce chloromethane as a solvent, refrigerant, or for syntheses of other chemicals. Hydrocyanic acid production via Andrussow or Degussa processes. Synthesis gas production via steam reforming, carbon disulfide production via methane reaction with sulfur over silica gel at 650 ˚C. In addition to mentioned chemicals, acetylene can be synthesized from methane in an electric arc at 2000 ˚C or via the Sachsse-Bartholome process [1].

The oxidative coupling of methane (OCM) comprises heterogeneous catalytic and homogeneous non-catalytic processes for converting methane mainly into C_2 hydrocarbons. Figure 2.1 represents a reaction network for OCM which was proposed by Baerns *et al*.

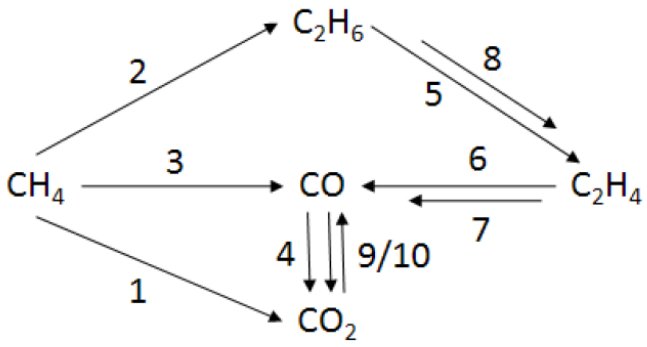

1: $CH_4 + 2\ O_2 \longrightarrow CO_2 + 2\ H_2O$
2: $2CH_4 + 0.5\ O_2 \longrightarrow C_2H_6 + H_2O$
3: $CH_4 + O_2 \longrightarrow CO + H_2O$
4: $CO + 0.5\ O_2 \longrightarrow CO_2$
5: $C_2H_6 + 0.5\ O_2 \longrightarrow C_2H_4 + 2\ H_2O$
6: $C_2H_4 + 2\ O_2 \longrightarrow 2\ CO + 2\ H_2O$
7: $C_2H_4 + 2\ H_2O \longrightarrow 2\ CO + 4\ H_2$
8: $C_2H_6 \longrightarrow C_2H_4 + H_2$
9/10: $CO + H_2O \longrightarrow CO_2 + H_2$

Figure 2.1. Reaction scheme and pathways from [8].

To obtain reasonable yields of C_2 hydrocarbons (C_2H_6 and C_2H_4), the reaction must be controlled kinetically. For this purpose, suitable catalysts are necessary. However, the known catalysts are not very active at low temperatures, thus the reaction requires temperatures

between 700-900 ˚C, which leads to low yields (due to consecutive CO_x formation) and severe catalyst deactivation (due to decomposition or sintering, caused by the high reaction temperatures) [7].

In particular, at temperatures from 677 to 927 ˚C which are typical for the OCM reaction, homogeneous processes mainly control the coupling reaction [9]. Hence, at very high temperatures, the yield of hydrocarbons is limited irrespective of the amount of catalytically active sites and hence methyl radicals. Therefore, a high-performance OCM catalyst should not only initiate the formation of CH_3 radicals at lower temperatures but also suppress nonselective surface oxidation of methane and hydrocarbon products to carbon dioxide. The required multi-functionality of a catalyst could be the reason why a multitude of oxide solids with different solid-state properties show activity in the OCM reaction. The catalytic materials can be classified into four groups [10]:

(i) Reducible metal oxides ($Sr_{0.75}Na_{0.25}NiO_{3-x}$, $SrMnO_x$, and $SrCoO_{x)}$
(ii) Non-reducible metal oxides (Li/MgO, $Mn/Na_2WO_4/SiO_2$, La_2O_3, and $NaMnO_4$/MgO)
(iii) Halogen-containing oxide materials ($CaCl_2$/CaO, an BaF_2/Y_2O_3)
(iv) Solid electrolytes ($SrCe_{0.9}Yb_{0.1}O_x$)

The Li/MgO catalyst is one of the most extensively studied catalysts in literatures; for the OCM reaction as it shows high catalytic activity in the low temperature range. However, Li/MgO and many other catalysts still could not achieve a C_2 yield beyond 25% and a selectivity of C_2 higher than 80% in a single-pass mode[11]. There are lots of questions which must be answered; questions like active centers, maximum solubility of Li in the MgO lattice, the position and nature of Li in the MgO, the stability of the catalyst, and many other questions are not still addressed [12].

2.1. Preparation of Li/MgO Catalyst

2.1.1. Wet Impregnation Method

Lithium promoted MgO catalysts (Li/MgO) were prepared by adding MgO and Li_2CO_3 to deionized water and evaporating the water, while stirring, until only a thick paste

remained. This paste ($Li_2CO_3/Mg(OH)_2$) was dried at 140 ˚C for a 5 h and then transformed to Li promoted MgO by passing 0.83 ml s^{-1} of oxygen for 1 h at 465 ˚C [4].

Lithium doped MgO (Li/MgO=0.1) catalysts were also prepared by completely mixing powdered precursors of Li_2O (including $LiNO_3$, CH_3COOLi, and Li_2CO_3) and precursors of MgO (including $Mg(NO_3)_2$, $(CH_3COO)_2Mg$, $MgCO_3$, MgO, and $Mg(OH)_2$ which is prepared using different magnesium salts and precipitation agents) in deionized water just enough to form a thick paste. Resulted paste then was dried at 120 ˚C for 4 h and calcined at 750 ˚C for 6 h which finally crushed, pressed and sieved to 22-30 mesh size particles. A comparison between different precursors and their effect on final results are provided in Table 2.1 [13].

In another work, Matsura *et al.* added Li_2O to a suspension of ultra-fine crystalline MgO in C_2H_5OH; resulted suspension were dried at 78 ˚C and calcined at 740 ˚C for 4 h. They showed that using this method for Li/MgO catalyst preparation resulted in exceptionally high activity for the OCM [14].

Arndt *et al.* mixed MgO and Li_2CO_3 in distilled water and then evaporated to get a thick paste. After overnight drying at 140 ˚C and calcining in air at 465 ˚C for 1 h, catalyst crushed and sieved, to obtain only particles smaller than 200 μm for catalytic studies [15].

Table 2.1. OCM over Li/MgO catalysts prepared using various precursors for Li_2O and MgO (reaction conditions: CH_4/O_2 = 8.0 and GHSV = 5140 $cm^3\ g^{-1}\ h^{-1}$). Reproduced with permission from [13] via Copyright Clearance Center.

Catalyst code	**Precursor**		**Temperature 650˚C**		**Temperature 750˚C**		**$MgCO_3$ phase in catalyst**
	For Li_2O	For MgO	X_{CH4} (%)	Y_{C2} (%)	X_{CH4} (%)	Y_{C2} (%)	
A	$LiNO_3$	$Mg(OH)_2$ (I)[a]	4.3	2.4	19.1	14.8	Nil
B	CH_3COOLi	$Mg(OH)_2$ (I)[a]	3.7	1.4	20.1	14.2	Minor
C	Li_2CO_3	$Mg(OH)_2$ (I)[a]	4.2	2.1	18.4	13.9	Minor
D	Li_2CO_3	$Mg(OH)_2$ (II)[b]	3.1	1.8	17.2	13.4	Trace
E	Li_2CO_3	$Mg(OH)_2$ (III)[c]	6.8	3.9	19.0	14.3	Minor
F	Li_2CO_3	$Mg(OH)_2$ (IV)[d]	3.9	2.4	15.1	11.1	Trace
G	Li_2CO_3	$Mg(OH)_2$ (V)[e]	0.9	0.5	7.1	5.5	Trace
H	Li_2CO_3	$Mg(OH)_2$ (VI)[f]	3.4	1.7	16.3	12.5	Trace
I	Li_2CO_3	$MgCO_3$	5.6	3.5	21.9	16.7	Minor
J	$LiNO_3$	$MgCO_3$	5.6	3.5	20.5	15.9	Minor
K	CH_3COOLi	$MgCO_3$	7.2	4.5	21.1	16.4	Minor
L	Li_2CO_3	MgO	4.4	2.9	17.8	13.7	Trace
M	CH_3COOLi	$(CH_3COO)_2Mg$	8.8	5.7	21.0	15.8	Minor
N	$LiNO_3$	$Mg(NO_3)_2$	4.8	2.4	20.8	14.9	Nil
For explanations of footnotes, and superscripts consult to the original paper							

2.1.2. Sol-gel Method

Lopez *et al.* prepared MgO gel using $Mg(OEt)_2$ which was refluxed with water and ethanol under constant agitation. They used hydrochloric acid, acetic acid, oxalic acid, and

ammonium hydroxide as a hydrolysis catalyst. This solution was kept at reflux and under constant agitation until it geled (89 h for HCl, 48 h for CH_3COOH, 67 h for $H_2C_2O_4$, and 21 h for NH_4OH). Resulted product was dried at 70 ˚C for 12 h and a final heat treatment at various temperature was done. ($Mg(OEt)_2$ was prepared by constant agitation of metallic Mg with anhydrous ethyl alcohol and iodine. The reaction continued for 24 h while adding some more ethanol to make sure that all Mg metal particles were reacted). This method and conventional wet impregnation method compared and it was shown that Li/MgO catalysts prepared via sol-gel method had comparable activities to Li/MgO catalysts prepared by wet impregnation of commercial MgO, but substantially higher C_2 selectivities [16, 17].

Trionfetti *et al.* synthesized high surface area nano-scale Li/MgO by adding 0.8 M methanol solution in water (as a gelation agent) to a mixture of 8.7 wt.% $Mg(OCH_3)_2$ in methanol and desired amount of $LiNO_3$ (to obtain 1, 3, and 5 wt.% Li in MgO) at room temperature. Resulted solution allowed to stand for 24 h for gelation (wet gels). After drying at 50 ˚C in vacuum for 7 h and thermal treatment at 500 ˚C the catalyst used as an efficient catalyst for olefins from methane. Authors proposed that sol-gel method eased incorporation of appreciable amount of lithium into the magnesia gel during catalyst preparation and retained in the oxide matrix after gel thermal treatment. Furthermore, limiting the presence of free lithium, preventing associated sintering, and loss of surface area are considered as other advantages of using sol-gel method [18].

2.1.3. Other Methods

2.1.3.1. Supported Li/MgO catalyst. Choudhary *et al.* synthesized Li/MgO supported on conventional supports, such as Al_2O_3, ZrO_2, HfO_2, SiC, and SiO_2 containing materials. Conversion and selectivity were approximately reduced by a factor of 3, compared to unsupported Li/MgO. This results were attributed to the reduction of the surface basicity, which could be an effect of a strong interaction of the catalyst material with the support. With Al_2O_3, SiO_2, and ZrO_2, the formation of mixed oxides containing Li or MgO was found, indicating that these materials are not suitable as inert carriers [19].

2.1.3.2. Precipitation. Arndt *et al.* prepared an aqueous solution of $Mg(NO_3)_2$ by dissolving $Mg(NO_3)_2 \times 6H_2O$ in distilled water. Produced solution slowly added to ammonia solution

while stirring and keeping pH value above 11. Precipitated $Mg(OH)_2$ was rinsed with distilled water and mixed with LiOH solution which is prepared in desired concentration in a tubular mixer. Final solution was quick frozen using liquid nitrogen and it was freeze-dried over 72 h. After calcination at 900 ˚C for 1h in a MgO crucible and crushing and sieving particles smaller than 200 μm were used [15].

2.1.3.3. Mixed Mill. Based on its easiness and fastness; this method is suited for industrial applications. $LiNO_3$ and MgO were milled in a centrifugal ball mill for 1 h at 400 round min^{-1} with alternating directions. Afterwards, the prepared samples were calcined at 400 ˚C for 3 h; resulted material crushed and sieved and particles less than 200 μm were used [15].

2.1.3.4. Chemical Vapor Deposition. Berger *et al.* used metal vapors of magnesium and lithium with oxygen to prepare Li-doped MgO nanoparticles. A cylindrical furnace was used with concentric inner stainless steel tube and outer quartz tube. Vaporized magnesium and lithium (desired amount) were mixed inside the stainless steel tube and combusted at the end of reactor with oxygen which came from outer quartz tube and collected within a stainless steel net. Analysis of before and after annealing under high vacuum conditions revealed that about 50% of the introduced Li was lost during activation via evaporation. They showed that Li+ ions preferentially moved into surface sites associated with low-coordinated ions and improved surface reactivity [20].

2.1.3.5. Gel Combustion Method. Zavyalova *et al.* synthesized lithium doped magnesium oxide using gel combustion method. Different lithium loadings was prepared by thermal ignition of the Mg and Li nitrates in a mixture of glycerol and ethanol and subsequently calcination at 800 ˚C for 2 h [21]. They have reported a detailed morphological study on this catalyst.

2.2. Performance and Stability Study of Li/MgO Catalyst

Procedures and conditions need to be met for effective utilization of a catalyst in a fixed bed reactor in order to a get a continuous and longtime activity and selectivity. Li/MgO is among the catalysts, which often used for strongly exothermic reaction of OCM and loses its activity and selectivity gradually. Taniewski *et al.* investigated the effective utilization of

the catalyst bed for OCM; results presented in their work, confirmed that; hot spots were only working regions of the bed and the region of the ageing of the Li/MgO catalyst. Under applied conditions, a gradual decrease in activity and selectivity of Li/MgO catalyst was observed. They confirmed that different layers with different activities and selectivities along the catalyst bed were formed. Elimination of less selective aged parts of the bed from the participation in the process and utilization of all fresh parts in the process, was introduced as a solution for this problem. Proposed solution can be applied by feeding the bed from different inlet locations parallel to the progress of ageing, see the Figure 2.2. The probability of absorbance of escaped lithium from the working catalyst by aged catalyst (in the case of Li/MgO catalyst) is also discussed [22].

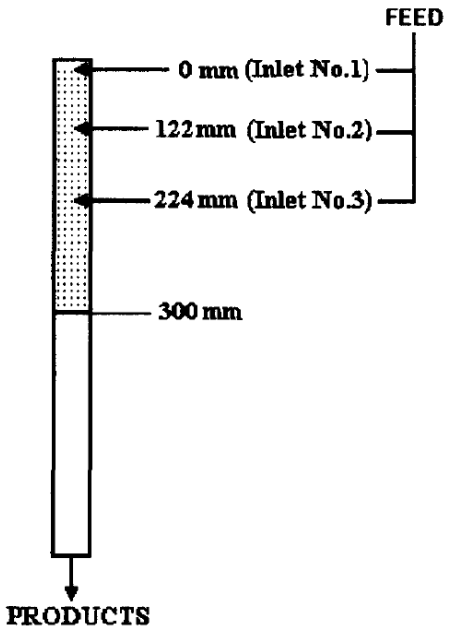

Figure 2.2. Schematic of reactor with various feed inlets. Reprinted with permission from [22] via Copyright Clearance Center.

Lithium loadings of 0, 0.5, 1, 2, 4, and 8 wt.% using four different preparation techniques with detailed AAS, BET, XRD, solid state NMR, SEM, and TEM test were employed to see the effect of Li loading and preparation technique on the stability of lithium doped magnesium oxide [15]. All catalyst showed a severe activity and selectivity decrease during first hour of reaction and a milder decrease through the 24 h stability test. No correlation were reported between activity, Li-loading, specific surface area, and grain size. Because of strong deactivation, loss of Li and its effect on reactor materials, Li/MgO was

not considered as a promising catalyst for OCM. Figure 2.3 shows lithium content versus OCM reaction time for differently prepared 0.5 wt.% Li/MgO catalyst. Disregarding of initial Li loading in the catalyst and preparation procedure, Li residual content falls to 0.01-0.03 wt.% after 7 h of reaction and remains constant until the end of reaction.

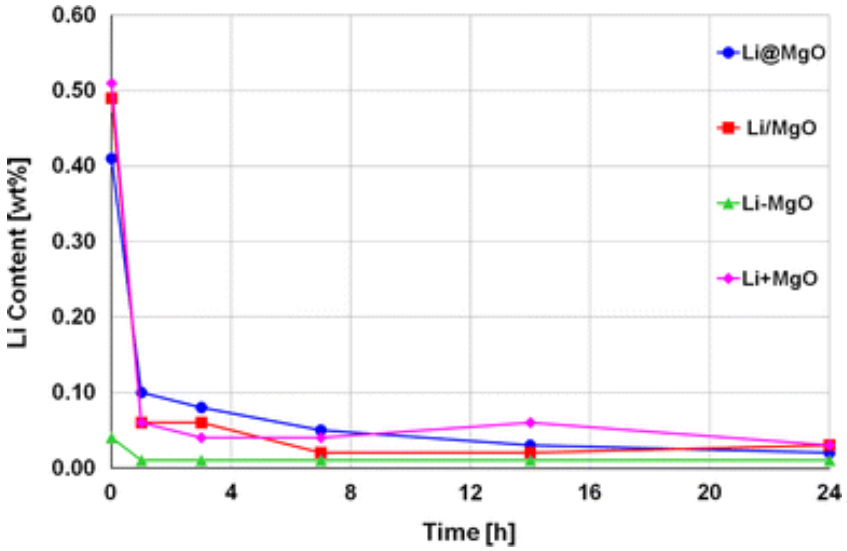

Figure 2.3. Loss of Li versus time during OCM reaction for differently prepared catalysts (Li@MgO: single source precursor, Li/MgO: wet impregnation, Li-MgO: precipitation, Li+MgO: mixed mill). Reprinted with permission from [15] via Copyright Clearance Center.

Table 2.2 provides a nice summary of different reaction conditions and catalytic results which were adapted with permission from Arndt *et al.* [12]. Recently Arndt *et al.* has reviewed almost all papers in the field of Li doped magnesium catalyst and they believe that because of varying reaction conditions and large amount of inert diluent used in the feed gas; a comparison is not possible. Li doping over MgO reduces its surface area; Kuo *et al.* showed that lost surface area could be compensated by addition of charcoal at the preparation step [23]. Charcoal was converted to CO_2 and increased the porosity of the catalyst but at the same time inhibited the formation of large MgO crystals. There was no correlation between specific surface area and the catalyst selectivity and conversion. They concluded that residence time had affected the previous studies which had concluded that BET surface area is determining the activity. They proposed a correlation between methane conversion and the total area in the reactor, also they proposed a reverse correlation between catalyst density and specific surface area of the catalyst.

Table 2.2. Overview of the reaction conditions and catalytic performance taken from selected publications. The difference between C_2 and C_{2+} selectivity which is usually small, has been neglected and reported as C_2. Gas hour space velocity (GHSV) was calculated according to the formula GHSV = Flow rate / mass of catalyst. Adapted with permission from Table 2.1 of [12] via Copyright Clearance Center.

No.	**Catalyst**	**Mass**	**CH_4:O_2: diluent**	**Temp.**	**Flow rate ml min^{-1}**	***X*** **$_{CH4}$ [%]**	***X*** **$_{O2}$ [%]**	***S*** **$_{C2}$ [%]**	**C_2H_6/ C_2H_4**	**GHSV ($cm^3\,g^{-1}_{cat}\,h^{-1}$)**	**Comment**	**Ref.**
1	7 wt.%	4.000 g	1.9:1:3.6	720 °C	49.8	37.5	n.s.	46.5	0.48	747	—	[24],[4]
2	8 wt.%	0.800 g	2.1:1:17.5	700 °C	55.2	22.6	n.s.	56.7	—	4140	—	[4]
3	4.8 wt.%	4.000 g	5.1:1 6.2	700 °C	50.0	14.6	n.s.	57.4	—	750	After10h	[25]
4	4.5 wt.%	4.000 g	5.1:1:6.2	700 °C	50.0	13	n.s.	58.9	—	750	After10h	[25]
5	5.5 wt.%	4.000 g	5.1:1:6.2	700 °C	50.0	20.3	n.s.	59.6	—	750	After10h	[25]
6	1.3 wt.%	2.000 g	2:1:2	760 °C	50.0	37	n.s.	40	0.25	1500	—	[26]
7	1.3 wt.%	2.000 g	2:1:2	780 °C	50.0	37	n.s.	40	0.21	1500	—	[26]
8	1.3 wt.%	2.000 g	2:1:2	800 °C	50.0	37	n.s.	40	0.18	1500	—	[26]
9	3.1 wt.%	0.093 g	9.6:1:3.7	780 °C	25.2	13.3	100	73	0.72	16451.6	—	[27]
10	0.63 wt.%	2.000 g	5.5:1:5.5	750 °C	—	25.2	100	41.9	1.00	—	—	[28]
11	1 mol%	0.100 g	3:1:0	700 °C	50.0	38.5	94.8	49	0.52	30000	—	[14]
12	3 mol%	0.100 g	3:1:0	700 °C	50.0	38.3	91.4	55	0.51	30000	—	[14]
13	5 mol%	0.100 g	3:1:0	700 °C	50.0	30.4	68.4	54.1	0.54	30000	—	[14]
14	10 mol%	0.100 g	3:1:0	700 °C	50.0	16.1	43.4	56.2	0.61	30000	—	[14]
15	15 mol%	0.100 g	3:1:0	700 °C	50.0	5.8	12.8	54	0.67	30000	—	[14]
16	Li/Mg = 0.1	0.100 g	3:1:0	750 °C	17.0	28.7	n.s.	63.1	0.91	10200	Code A	[13]
17	Li/Mg = 0.1	0.100 g	3:1:0	750 °C	17.0	22.1	n.s.	59.7	1.25	10200	Code B	[13]
18	Li/Mg = 0.1	0.100 g	3:1:0	750 °C	17.0	24.8	n.s.	56.9	1.25	10200	Code C	[13]
19	Li/Mg = 0.1	0.100 g	3:1:0	750 °C	17.0	19.7	n.s.	65	1.25	10200	Code D	[13]
20	Li/Mg = 0.1	0.100 g	3:1:0	750 °C	17.0	33.5	n.s.	55.8	0.71	10200	Code E	[13]

Table 2.2. Overview of the reaction conditions and catalytic performance taken from selected publications. The difference between C_2 and C_{2+} selectivity which is usually small, has been neglected and reported as C_2. Gas hour space velocity (GHSV) was calculated according to the formula GHSV = Flow rate / mass of catalyst. Adapted with permission from Table 2.1 of [12] via Copyright Clearance Center (cont.).

No.	Catalyst	Mass	CH_4:O_2: diluent	Temp.	Flow rate ml min^{-1}	X_{CH4} [%]	X_{O2} [%]	S_{C2} [%]	C_2H_6/ C_2H_4	GHSV ($cm^3\,g^{-1}_{cat}\,h^{-1}$)	Comment	Ref.
21	Li/Mg = 0.1	0.100 g	3:1:0	750 °C	17.0	18.6	n.s.	30.6	2.00	10200	Code F	[13]
22	Li/Mg = 0.1	0.100 g	3:1:0	750 °C	17.0	6.6	n.s.	66.6	3.33	10200	Code G	[13]
23	Li/Mg = 0.1	0.100 g	3:1:0	750 °C	17.0	21.8	n.s.	59.6	1.43	10200	Code H	[13]
24	Li/Mg = 0.1	0.100 g	3:1:0	750 °C	17.0	31.7	n.s.	59	0.63	10200	Code I	[13]
25	Li/Mg = 0.1	0.100 g	3:1:0	750 °C	17.0	29.6	n.s.	59.1	0.77	10200	Code J	[13]
26	Li/Mg = 0.1	0.100 g	3:1:0	750 °C	17.0	36.1	n.s.	60.1	0.59	10200	Code K	[13]
27	Li/Mg = 0.1	0.100 g	3:1:0	750 °C	17.0	25.1	n.s.	64.9	0.77	10200	Code L	[13]
28	Li/Mg = 0.1	0.100 g	3:1:0	750 °C	17.0	38	n.s.	55.3	0.42	10200	Code M	[13]
29	Li/Mg = 0.1	0.100 g	3:1:0	750 °C	17.0	24.5	n.s.	52.2	1.25	10200	Code N	[13]
30	Li/Mg = 0.1	0.500 g	4:1:0	750 °C	86.0	11.9	n.s.	50	3.33	10320	—	[29]
31	Li/Mg = 0.1	0.500 g	4:1:0	750 °C	86.0	27.6	n.s.	64	1.18	10320	—	[29]
32	0.66 wt.%	0.093 g	10:1:0	780 °C	25.2	4.4	50	66.4	1.37	16258.1	—	[30]
33	1.71 wt.%	0.093 g	10:1:0	780 °C	25.2	10	75	75.1	75.1	16258.1	—	[30]
34	2.47 wt.%	0.093 g	10:1:0	780 °C	25.2	11.1	85	71.7	1.12	16258.1	—	[30]
35	3.19 wt.%	0.093 g	10:1:0	780 °C	25.2	11.4	88	72	1.24	16258.1	—	[30]
36	0.02 wt.%	2.000 g	3.7:1:17.4	650 °C	50.0	4.1	n.s.	7.6	—	1500	—	[31]
37	0.05 wt.%	2.000 g	3.7:1:17.4	650 °C	50.0	6.2	n.s.	9.6	—	1500	—	[31]
38	0.10 wt.%	2.000 g	3.7:1:17.4	650 °C	50.0	7.6	37.0	17.5	—	1500	—	[31]
39	0.15 wt.%	2.000 g	3.7:1:17.4	650 °C	50.0	9.3	44.4	25.7	—	1500	—	[31]
40	0.20 wt.%	2.000 g	3.7:1:17.4	650 °C	50.0	8.2	38.3	35.7	—	1500	—	[31]

Table 2.2. Overview of the reaction conditions and catalytic performance taken from selected publications. The difference between C_2 and C_{2+} selectivity which is usually small, has been neglected and reported as C_2. Gas hour space velocity (GHSV) was calculated according to the formula GHSV = Flow rate / mass of catalyst. Adapted with permission from Table 2.1 of [12] via Copyright Clearance Center (cont.).

No.	Catalyst	Mass	CH_4:O_2: diluent	Temp.	Flow rate ml min^{-1}	X_{CH4} [%]	X_{O2} [%]	S_{C2} [%]	C_2H_6/ C_2H_4	GHSV	Comment	Ref.
41	0.25 wt.%	2.000 g	3.7:1:17.4	650 °C	50.0	9.6	36.8	30.8	—	1500 $cm^3 g^{-1}_{cat} h^{-1}$	—	[31]
42	1.00 wt.%	2.000 g	3.7:1:17.4	650 °C	50.0	9.1	44.8	36.4	—	1500 $cm^3 g^{-1}_{cat} h^{-1}$	—	[31]
43	5.00 wt.%	2.000 g	3.7:1:17.4	650 °C	50.0	8	30.4	34.5	—	1500 $cm^3 g^{-1}_{cat} h^{-1}$	—	[31]
44	7.00 wt.%	2.000 g	3.7:1:17.4	650 °C	50.0	6	27.4	30.6	—	1500 $cm^3 g^{-1}_{cat} h^{-1}$	—	[31]
45	10.00 wt.%	2.000 g	3.7:1:17.4	650 °C	50.0	7.6	n.s.	35.6	—	1500 $cm^3 g^{-1}_{cat} h^{-1}$	—	[31]
46	0.2 %	4 ml	3:1:0	700 °C	75.5	29.8	94.2	58.8	2.40	1133 ml $ml_{cat}^{-1} h^{-1}$	—	[32]
47	2.0 %	4 ml	3:1:0	700 °C	85.7	22.1	63.9	62.8	1.54	1286 ml $ml_{cat}^{-1} h^{-1}$	—	[32]
48	5.0 %	4ml	3:1:0	700 °C	88.0	11.8	27.8	53	2.27	1320 ml $ml_{cat}^{-1} h^{-1}$	—	[32]
49	5 %	4 ml	3.3:1:0	720 °C	43.2	2.7	n.s.	65.4	0.65	648 ml $ml_{cat}^{-1} h^{-1}$	—	[33]
50	5 %	4 ml	3.3:1:0	550 °C	43.2	1.6	n.s.	22.5	3.5	648 ml $ml_{cat}^{-1} h^{-1}$	—	[33]
51	0.6 %	1.25 ml	2:1:7.1	680 °C	50.0	38	n.s.	35	0.59	2400 ml $ml_{cat}^{-1} h^{-1}$	after 10 h	[34]
52	1.2 %	1.25 ml	2:1:7.1	680 °C	50.0	30	n.s.	41	0.71	2400 ml $ml_{cat}^{-1} h^{-1}$	after 10 h	[34]
53	4 wt.%	3.000 ml	2:1:6.3	700 °C	74.0	34.4	n.s.	46.7	0.46	1480 ml $ml_{cat}^{-1} h^{-1}$	after30 min	[35]
54	0 wt.%	0.100 g	4:1:4	750 °C	60	15.6	69.8	29.0	1.4	36000 $cm^3 g^{-1}_{cat} h^{-1}$	mix-mill 40 h	[15]
55	0.5 wt.%	0.100 g	4:1:4	750 °C	60	12.8	52.0	32.2	1.6	36000 $cm^3 g^{-1}_{cat} h^{-1}$	mix-mill 40 h	[15]
56	1 wt.%	0.100 g	4:1:4	750 °C	60	7.4	29.2	30.1	2.6	36000 $cm^3 g^{-1}_{cat} h^{-1}$	mix-mill 40 h	[15]
57	2 wt.%	0.100 g	4:1:4	750 °C	60	4.2	15.2	30.7	4.0	36000 $cm^3 g^{-1}_{cat} h^{-1}$	mix-mill 40 h	[15]
58	4 wt.%	0.100 g	4:1:4	750 °C	60	2.9	8.9	33.0	5.5	36000 $cm^3 g^{-1}_{cat} h^{-1}$	mix-mill 40 h	[15]
59	8 wt.%	0.100 g	4:1:4	750 °C	60	2.2	10.2	25.1	6.1	36000 $cm^3 g^{-1}_{cat} h^{-1}$	mix-mill 40 h	[15]
n.s., not specified												

The OCM was carried out without using a catalyst in a continuous flow at pressures ranges up to 10 bar, temperatures from 677 ˚C to 957 ˚C, and inlet molar ratios of CH_4/O_2 down to 2.5. The conversions of methane and oxygen increased substantially with increasing pressure at constant temperature and residence time. The STY of the C_2 products reached a level comparable to that required for industrial operations from 4 bar on. 38 elementary reactions were used to describe the experimental data. It was concluded that general features of the reaction mechanism do not depend on the total pressure. Methyl and hydrogen peroxy radicals were the most observed radicals. By increasing the total pressure, drastic increase in the concentrations of the chain carriers, particularly the hydrogen peroxy radical was observed. Higher pressures favored the oxidative route from ethane to ethylene compared to the pyrolytic route. Increasing the total pressure leads to an increase of the primary and a decrease of the consecutive CO formation relative to the coupling. The balance between these nonselective routes determines the effect of the total pressure on the integral selectivity to C_2 products at different conversions. [36].

Ekstrom *et al.* did a study on pressure effect in OCM reaction [37]. They concluded following points;

- Increasing pressure increases the reaction rate rapidly for blank reactor while this effect can be overcome by working at higher linear velocities
- Blank reaction and catalyzed reaction follow different routes by pressure change which results in blank reaction to be dominant at high pressures and low linear velocities
- Because of CO_2 poisoning at higher pressures, activity of catalysts (Li/MgO, Sm_2O_3, and Sr/Sm_2O_3) declines. Working at Higher linear velocities is proposed to counteract this effect.
- The only catalytic effect at higher pressures and lower linear velocities (<15 cm s^{-1}) is only CO converting to CO_2
- C_2 selectivity of the catalyst decreases with increasing linear velocity which can be related to the higher oxygen concentration present at the surface of the catalyst

Using quartz reactor for OCM had a negative effect on the stability of Li/MgO catalyst, because catalyst deactivates through the loss of Li as LiOH and/or Li_2SO_3 [7].

2.3. Engineered OCM

Fluidized bed and fixed bed reactors were used to investigate the OCM reaction. Fixed bed reactor gave encouraging results, but methane conversion was limited to 15%. By contrast, the fluidized bed reactor operated essentially isothermally at methane conversions in excess of 40% using methane/oxygen mixture (without diluent) well inside the explosive limits. Agglomeration problems were seen at lithium content higher than 0.4 wt.% [38] .

Alonized 316 stainless steel reactors were tested using Li/MgO catalyst. severe corrosion of the portion of the reactor in contact with the catalyst bed demonstrated that Alonized 316 stainless steel reactor is unsuitable for use in methane coupling service using Li/MgO catalyst[39].

Ethane co-feeding greatly increases methane conversion in the absence of catalyst. This happens as a result of lower C-H bond energy in ethane which increases the propagation rate and thus increases the branching rates in a branched-chain mechanism. Co-feeding of ethane for OCM using Sn/Li/MgO as a catalyst has no beneficial effect [40].

Heat produced from exothermicity of the OCM and side reactions cannot be effectively removed through the wall of a tubular reactor. This fact, along with poor heat transfer along the bed, leads to hot spots formation in the bed. Dilution of the catalyst in a fixed bed reactor with properly chosen inert solid diluent, admixed in such proportions that the amount of active component remains sufficient, may lead to some improvements of heart transfer of the fixed bed area. Quartz chips have detrimental effect while α-Al_2O_3 seems promising candidates to be added as a diluent of Li/MgO catalyst's bed [41].

OCM was simulated for different membrane reactors; i.e. porous membrane reactor (PMR), mixed ionic and electronic conducting membrane reactor (MIEMR), and solid oxide fuel cell reactor (SOFCR) and then was compared to fixed bed reactor. Kinetic expressions of Li/MgO catalyst were employed in FBR, PMR, and MIEMR models. Model showed that

FBR was not recommended for OCM whereas PMR and MIEMR were suitable at temperatures lower than 877 ˚C and higher than 877 ˚C, respectively. Impurities in PMR feed was forbidden. MIEMR and SOFCR showed promising performance at higher pressures. Higher temperatures were needed for SOFCR (approximately 200K) in comparison to the other reactors and methane loss through the non-selective porous membrane were some predicted drawbacks of these system[42]. C_2 yield of 18.4 at selectivity of 60% was observed for a LaSr/CaO modified BSCFO ($Ba_{0.5}Sr_{0.5}Co_{0.8}Fe_{0.2}O_{3-v}$) membrane reactor. The best performance was reported at 950 ˚C [43].

Classically heated coupled with microwave irradiated reactor was investigated by Roussy *et al.* to see its effect on OCM reaction over Li/MgO and $BaBiO_{3-x}$ catalysts [44]. Improved C_2 selectivity was reported for Li/MgO and a negligible improvement for $BaBiO_{3-x}$. This behavior can be explained by the catalytic oxidation rate of methyl radicals into CO and CO_2. Quenching of products and electromagnetic field (which decreased the surface oxygen concentration), both resulted in lower oxidation rates of $CH_3^{\cdot}$ In the gas phase and consequently higher C_2 selectivities. It should be considered that these results are applicable at lower temperatures (650 ˚C) where the yield increased from 2% to 8%.

Ross *et al.* studied the process conditions on OCM in an engineered manner and they concluded following rules [45];

- O_2 concentration in the feed must be kept at lower levels or CH_4/O_2 ratio must be high to reach higher selectivities
- Gas phase reactions must be minimized because of its non-selective nature
- Plug flow conditions must be met to avoid products (C_2H_4 and C_2H_6) oxidation

2.4. Effect of Promoter on Li/MgO catalyst

Many promoters were investigated to improve Li/MgO catalyst, mainly to improve its stability. These attempts were generally in two directions; firstly, solid phase modification and secondly, shifting reaction conditions toward milder conditions [12].

It has shown that addition of small amounts of transition and/or rare earth metals can improve the activity and stability of lithium doped magnesium oxide in OCM reaction. Korft *et al.* investigated a number of different additives such as; SnO_2, Tb_4O_7, Dy_2O_3, and TiO_2 on OCM. They results showed that these additives have little or no improvements on the selectivity toward C_2 products while they substantially decreased the required temperature to reach optimum yields of C_2 products. They reported that La_2O_3 and NiO did not change the selectivity while improved conversion while CoO, MnO_2, PbO, and Bi_2O_3 decreased the temperature for a particular conversion. They studied different aspects of these catalysts such as: nature of phase presented in the calcined materials, decomposition of carbonate phase in the catalyst, the effect of promoter concentration, and the aging behavior under oxidative coupling conditions. Korft *et al.* introduced the Li/Sn/MgO as the most promising catalyst based on their evaluation criteria [46].

Larkins and Nordin investigated the effect of Li_2CO_3 being present in the preparation of Li/MgO, loaded with different amounts of ZnO and Manganese oxide in OCM. When Li_2CO_3 is excluded, carbon oxide production were favored. A conversion and selectivity of 25% and 60% was reached respectively using Li_2CO_3/MgO catalyst while changing the amount of Zn presented did not change the selectivity ore conversion at 805 ˚C. Loading small amounts of manganese oxide on Li_2CO_3/MgO catalyst resulted in methane conversions higher than 35% and C_2 selectivity near 50%. Higher loading values was not promising [47].

The zirconium effect on Li/MgO was studied by Ross *et al.* In this study, zirconia amount was fixed and different concentrations of lithium was tested. Initial activity was decreased by increasing the amount of lithium doped on Zr/MgO catalyst while selectivity remained unchanged. It was concluded that life-time of zirconium doped Li/MgO catalyst was a function of the lithium content. Instability of $Li_2Mg_3ZrO_6$ was shown in previous studies, in spite of this catalyst good activity and selectivity [48].

McNamara *et al.* investigated the effect of Nb_2O_5 or ZrO_2 on Li/MgO and Li/Na/MgO catalyst for optimal C_2 production from methane. Furthermore, a comparison between Nb_2O_5 or ZrO_2 and SnO_2 or Co_3O_4 promoted catalysts were also conducted. At temperatures less than 700 ˚C, the Li/Co/MgO ternary system showed the best performance in comparison to the other ternary candidates [49].

The effect of cerium promoted lithium doped magnesium oxide and lithium doped magnesium oxide-calcium oxide on OCM was investigated by Tiwari *et al.* in the presence of molecular oxygen at 730 ˚C [50]. They used impregnation method for catalyst preparation, calcined the catalyst at 900 ˚C and tested it at the CH_4/O_2 of 2. They found 7 wt.% Li - 2 wt.% Ce doped over MgO-CaO (with a rate ratio of 3) as the most promising catalyst with a methane single pass conversion of 28% and C_2 selectivity of 77%.

Investigations of Lunsford *et al.* on effect of Cl^- on Li/MgO catalyst in the OCM revealed that the catalyst performance extremely changes at a Cl^-/Li^+ ratio of one [51]. Production ratio of ethylene to ethane increased because of the improved activity toward oxidative dehydrogenation of ethane. Catalyst basicity increased by addition of Cl^- which inhibited the reaction of catalyst with CO_2 and formation of Li_2CO_3. Generally Li/Cl/MgO had a lower activity than pure Li/MgO catalyst. They reported that at 650 ˚C chlorine left the catalyst as HCl and a bit CH_3Cl.

2.5. OCM Mechanism over Li/MgO Catalyst

Lunsford *et al.* performed experiments similar to Abraham *et al.* using EPR spectroscopy. Relative intensity of EPR signals was correlated to methyl radical formation which were assigned to the concentration of the $[Li^+O^-]$. These correlation is shown in Figure 2.4 [52, 53].

Driscoll *et al.* showed that methyl radicals may be produced from MgO and Li doped MgO from methane. Their results suggests that oxygen anion is responsible for subtraction of hydrogen from methane and this oxygen anion is available in the form of $[Li^+O^-]$ center. They suggested that ethane probably is produced in the gas phase and as a result of methyl radicals coupling [53]. Based on their results they concluded that for lithium doped magnesium oxide, $[Li^+O^-]$ are active centers.

Ross *et al.* showed that catalysts with a high concentration of carbonates favored the production of ethylene and ethane. Catalysts which were calcined at lower temperatures had more CO_2 content and therefore showed better catalytic activity. They also concluded that

formation of active centers are a result of loss of carbonate species, which were unstable under the harsh reaction conditions of the OCM [54].

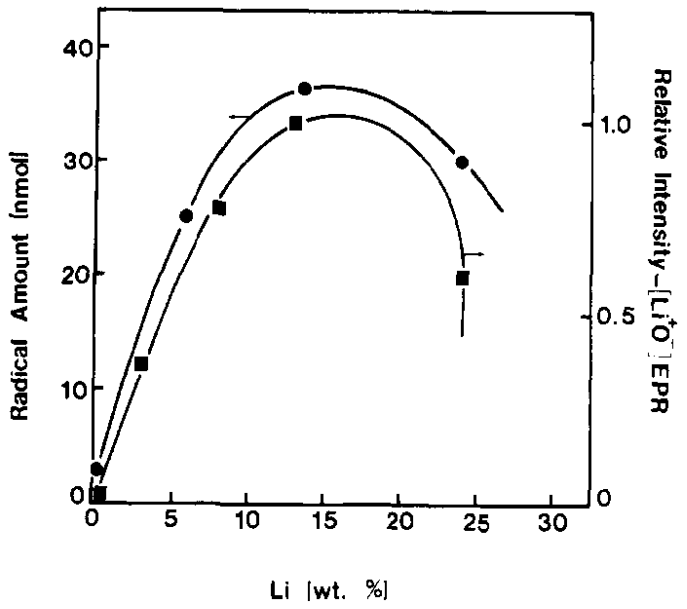

Figure 2.4. The amount of radicals and $[Li^+O^-]$ centers formed as a function of Li doping into MgO. T=500 ˚C, 0.5 g of catalyst, argon flow 3.8 cm^3 min^{-1}, CH_4 flow 1.14 cm^3 min^{-1}, O_2 flow 0.023 cm^3 min^{-1}. Preconditioned at 450 ˚C, 2.5 h, 300 cm^3 min^{-1} O_2. Reprinted with permission from [53] via Copyright Clearance Center.

Interaction of oxygen with the catalyst and its dissociative exchange between solid phase and gas phase was shown by Nibbelke *et al.*[55]. They also showed that doping the support material with Sn or Li increases the oxygen diffusion coefficient and as a result, its amount in the catalyst. C_2H_6 is the primary C_2 product in the OCM reaction, but oxidative dehydrogenation of C_2H_6 to C_2H_4 produces these product, in some cases, even more that ethane. Consecutive reactions were studied at low pressures (0.0001–0.015 bar) by Kasteren *et al.* who showed that C_2H_6 conversion (mainly to C_2H_4) was 4 times faster than CH_4. At the same time, C_2H_4 oxidized 2.6 times faster than CH_4 [56]. They suggest that reaching yield values higher than 25 and selectivities higher than 65% is possible if the interactions between heterogeneous and homogenous reactions are optimized.

Peng *et al.* investigated the surface composition and reactivity of Li/MgO catalyst kinetically and using XPS measurements. Under reaction conditions, they observed two Li containing phases in Li/MgO, consisted of $[Li^+O^-]$ and Li_2CO_3. The O (1s) XPS peaks were

assigned to the surface concentration of $[Li^+O^-]$. Correlation between CH_4 conversion and the concentration of surface $[Li^+O^-]$ reveals that the $[Li^+O^-]$ species is the active center for OCM. Moreover, they investigations suggests that saturation concentration of $[Li^+O^-]$ species happens at a Li loading of 0.2 wt.%. They presumed that higher loadings would evaporate from the surface and/or diffuse into the MgO. This findings are consistent with the discussion on the optimal loading of Li [57] and the experiments for the re-appraisal of the Li loading of Hutchings and co-workers [32].

Deactivation of the Lithium doped magnesium oxide was investigated by Mirodatos and co-workers [58]. They found following results:

(i) Catalyst sintering occurs through two different mechanisms
- Sintering via the liquid Li_2CO_3 phase at high temperatures
- Sintering under the influence of water and carbon dioxide through the reaction

(ii) Two different types of catalytic deactivation can occur with respect to the two sintering process.

(iii) The best catalytic performance was reached when a tight interface between Li_2CO_3 and MgO phases was reached, after a treatment allowing the liquefaction of the alkali salt.

On the basis of foregoing, the reaction mechanism shown in Figure 2.5 was proposed by Ekstrom and Lapszewicz [59].

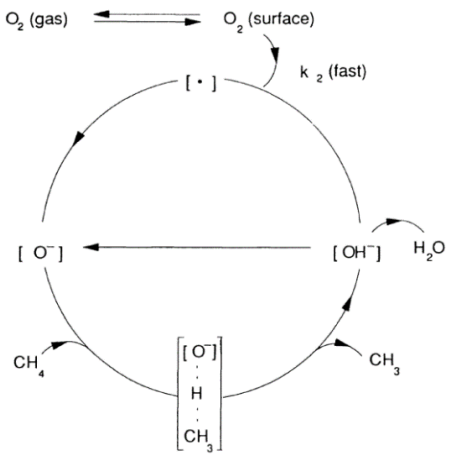

Figure 2.5. Reaction mechanism proposed by Ekstrom and Lapszewicz [59].

2.6. Monolithic Structures

Monolith in Greek language means “single stone”; mono stands for single and lithos stands for stone. Sometimes it could refer to honeycomb structure or in industrial terminology means the large uniform block of single building material. Based on monolith construction material it could be divided into metallic, plastic or ceramic monoliths[60]. Monolithic structure is produced using extrusion method with various clays, binders and additives. The most common clay is a mixture of alumina, magnesia, and silica which comprises 90% of all monolith catalysts used for conversion of toxic exhaust gases to more clean gases. Interests in this material for this application are related to its resistance to high temperatures and temperature shocks. Furthermore, it has really low thermal expansion which is favored for severe temperature applications [61].

Another important applications of the monoliths are selective catalytic reduction of off-gases produced by power stations and ozone destruction in airplanes. In spite of limited application of monoliths in industry, they show better performance than slurry and fixed bed reactors for multiphase reactions. Many operational advantages are counted for monolith catalyst such as: energy input, efficiency, safety, and catalyst preparation. There are also commercially available other materials made monolithic structures like silicon carbide, mullite ($3Al_2O_3.2SiO_2$), and metals. Disadvantage of all these material to be used as a support for catalytic applications are their low BET surface area (for cordierite typically 0.7 $m^2\ g^{-1}$). In order to increase BET surface area, a bare monolith can be coated with desired support; this procedure is commonly called wash-coating. Macro-porous structure of monolith surface eases the adhesion of support by anchoring mechanism. Wash coating is carried out in two different methods; first, high surface area support material is filled inside the macro-pores. Second, wash coat material can be deposited as a layer in ceramic support pores. This is shown schematically in Figure 2.6 [61].

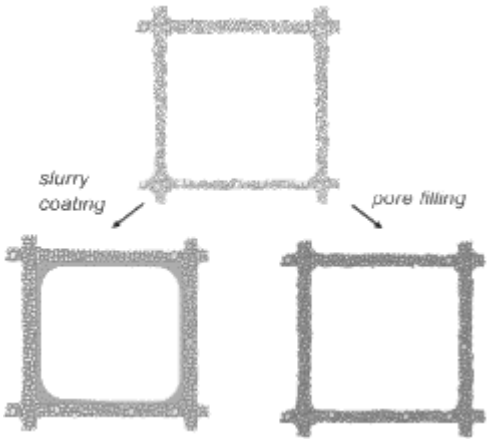

Figure 2.6. Representation of slurry coating and pore filling coating methods. Reprinted with permission from [61] via Copyright Clearance Center.

Monolithic catalysts have only one piece and there wouldn't be attrition due to moving particles. Furthermore, long straight forward channels results in extremely low pressure drop which both are favored in reactor design. Poor adhesion of support, low surface area, laminar flow through the channels, lack of interconnectivity between the channels, and terrible heat conduction in radial direction are considered disadvantages of monolithic catalyst. Higher residence time resulted from laminar flow in monolith channels decreases conversion [62].

One of the most important steps in monolithic catalyst preparation is active phase loading. Macroscopic redistribution of active phase precursor occurred during drying process of the monolith due to capillary suction results in accumulation of active metal in the outer shell of monolith. Therefore, finding methods to disperse and distribute active phase in a homogenous way is really crucial. Vergunst *et al.* conducted a study to determine preparation condition that ensures a uniform active phase distribution and find out non-uniform metal distribution reasons. They used Ni/Al_2O_3/Cordierite monolith system because distribution of active metal can be seen easily. Effect of nickel concentration, monolith drying method, and deposition-precipitation method was studied. Active phase metal immigration to the exterior surface must be prevented after it has been applied [63]. They proposed three methods to prevent the development of an inhomogeneous metal distribution;

(i) Formation of an insoluble catalyst precursor, by means of deposition precipitation
(ii) Use microwave heating to evaporate liquid throughout the monolithic structure
(iii) Use freeze-drying method to prevent liquid from flowing

Oxidative dimerization of methane over Li/MgO monolithic structure was studied by Aigler and Lunsford. Bare monolith and Li doped magnesium oxide monolithic structure are active catalysts for OCM. MgO monoliths are more active but less selective for the formation of ethylene and ethane. High activity of MgO attributed to Ca^{2+} impurities that was concentrated on the surface [34].

Perez-Cadenas *et al.* coated a cordierite ($2MgO.2Al_2O_3.5SiO_2$) monolith with α-Al_2O_3 using dip-coating method with the purpose of increasing surface area and blocking the macro-porous surface area of the monolith to prevent deposition of catalytic material. Bare monoliths were dipped in 70 wt.% α-Al_2O_3 (0.35-0.39 μm particles) in water suspension. The excess suspension in the channels was removed by flushing air flow and monoliths were dried at room temperature. Afterwards, monoliths were thermally treated to 1000 ˚C with a rate of 2 ˚C min^{-1} to avoid getting cracks and calcined at this temperature for 4 h. This monolith was ready to be impregnated with active metal or catalyst; Figure 2.7 shows first coating and third coating of monolith which resulted in round shape channels [64]. A direct comparison between different preparation techniques' performance is not possible because of vast varying testing conditions.

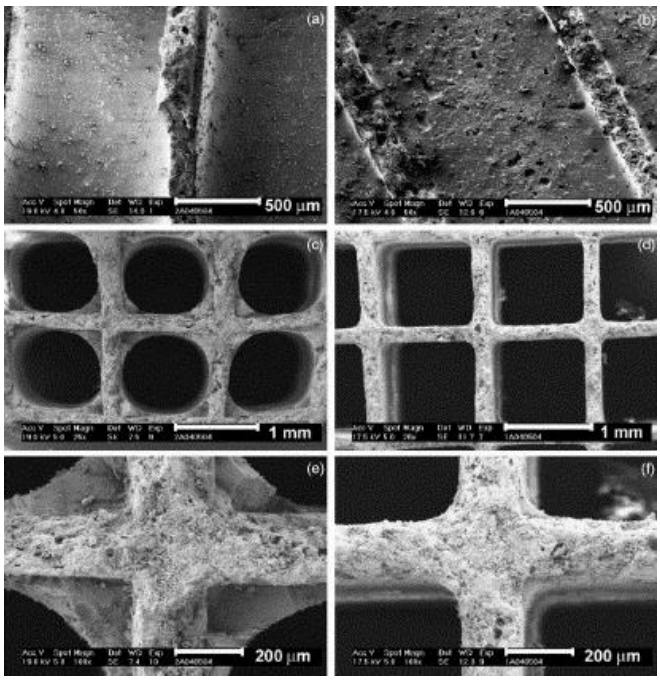

Figure 2.7. SEM images of the α-Al_2O_3 coated cordierite monolith after first dip-coating (b,d, and f) and third dip-coating (a,c, and e). Reprinted with permission from [64] via Copyright Clearance Center.

2.7. Summary

Hundreds of publications have been published about Li/MgO catalyst as a promising catalyst for OCM reaction until this day. Unfortunately, almost in 90% of the publications, the stability problem of the catalyst is neglected except for recent studies by Arndt *et al.* who investigated this catalyst considering this drawback. Therefore, catalytic activity is reported within the first few hours on stream when the catalyst is still fresh. Because of this fault and complexity of the heterogeneous-homogenous nature of OCM over Li doped MgO, almost no correlation was found to be consistent with general effective parameters on catalyst studies such as; specific surface area, acidity and basicity, temperature, lithium loading, effect of additives, pressure, and so on.

A large amount of diluent were used in those studies which reported Li/MgO as a stable catalyst whereas in direct utilization of methane and oxygen without diluent there was no any stable Li/MgO catalyst for OCM reaction. Also detection of lithium is not possible using EDX instrument because of its atomic number and scattered reflected X-ray from lithium containing material. There are enormous publications about oxidative coupling of methane over lithium doped magnesium oxide. Disregarding stability problem of this catalyst caused a lot of inconsistencies between papers.

In Arndt *et al.* experiments; analysis of residual lithium after 24 h time on stream revealed that only 0.01-0.03 wt.% Li remained in the catalyst [7], which is consistent with determined values by Anderson and Norby as thermodynamic solubility of Li in the MgO [65]. Arndt concluded that the loss of Li and the residual content of Li are independent of preparation technique.

3. MATERIALS AND METHODS

3.1. Experimental Setup

For the purpose of activity tests, a reaction system shown in Figure 3.1 were designed and constructed in the Catalysis and Reaction Engineering Laboratory of Chemical Engineering Department of Boğaziçi University. High purity reaction gases were passed through the stainless steel tubes and adjusted precisely with mass flow controller units which were calibrated specifically for desired gas. These gases were mixed and passed through the by-pass line for the purpose of feed analysis or through the reactor pass for the purpose of activity tests.

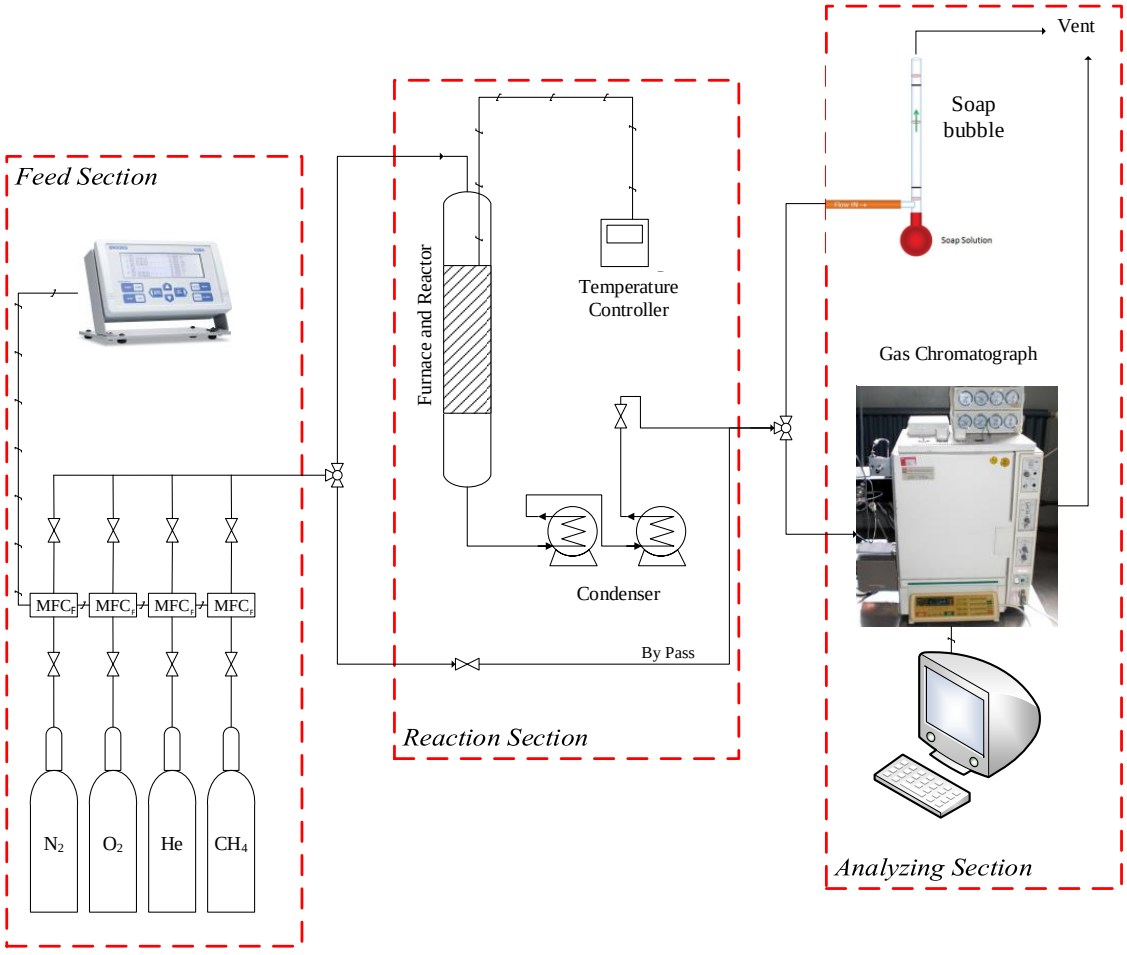

Figure 3.1. Feed, reaction and analyzing setup.

The highest temperature reachable by the electric furnace was 1000 ˚C which was controlled precisely by a Fp-21 programmable controller. Product gases were passed through two series of condenser to make sure no steam would go to the GC. A bubble meter was provided with a three way valve exactly before the GC to check leakage and do calibration for MFCs. Detailed specifications and explanations are provided for each operating part in the next sections. 4% nitrogen was used as internal standard to calculate volume shrinkage during the reaction. Total duration of each analysis was 50 min; 29 min for analysis and 21 min for cooling GC to its initial temperature. Therefore, every 50 min a data was taken for evaluation of activity, stability and selectivity; 8 data points in total.

3.1.1. Gas Analyzer

For the purpose of the feed and product gases analysis, a gas chromatography system was used. Detailed specification and set values for this apparatus can be found in Table 3.1.

Table 3.1. Gas analyzer specifications.

GC	Shimadzu GC 14A
Detector type	TCD
Column initial temperature	40 ºC
Column initial time	5 min
Column temperature increment rate	20 K min^{-1}
Column final temperature	220 ºC
Column finla time	15 min
Column injection temperature	220 ºC
Detector temperature	230 ˚C
Detector current	100 mA
Carrier gas	Helium
Carrier gas flow rate	30 ml min^{-1}
Column type	CBXN-1000 60/80
Column Length & ID	6 m, 2mm ID, 1/8 inch OD
Sample loop	2 mL
Sampling rate	100 ms

Different composition of each gas, balanced with He or other gases, were fed into the GC and calculated area vs. corresponding composition were linearized. Fitted equation for each gas then was used to calculate composition of each gas in the feed or product analysis. Calibration were done two times for oxygen and nitrogen; one for wide range concentrations and another for narrow range concentrations. This is done because nitrogen and oxygen peaks overlapped whereas the nitrogen was our internal standard and a small error in nitrogen composition would result in big errors in calculation of conversion and selectivity. Therefore, for the purpose of minimizing error, all probable compositions of these gases were calibrated.

Argon was tested as an internal standard candidate but the peak had same retention time of oxygen. Therefore, it has to be left out; second choice was to consider helium. Helium was not detected by the GC because it was GC carrier gas. On the other hand, sum of compositions must be one for both feed and product gases. Therefore, the composition of helium could be calculated from Equation 3.1 for feed and product gases.

$$X_{He} = 1 - \sum_{i=1}^{6} X_i \tag{3.1}$$

In the above equation X stands for gas composition and i stands for detected gases which were oxygen, carbon monoxide, methane, carbon dioxide, ethane, and ethylene. This method was not successful because OCM carried out at extremely high temperatures and the probability of not-detected gases production were high. On the other hand, each packed column is individually designed for particular gases and detection of unknown gases may not be possible for that specific packed column. As a result, the composition calculated for helium in the Equation 3.1 would be sum of not-detected gases which helium is one of them and could not be used as an internal standard.

Third choice was to use carbon balance method. Carbon mass balance is applied to determine flow rate of product gases. Input flow rate, input composition of carbon and output composition of carbon species (CO, CO_2, CH_4, C_2H_4, and C_2H_6 which are calculated by GC) are in hand. Total flow of product gases were calculated using Equation 3.2.

$$F_{out} = \frac{F_{in} \times X_{CH4_{in}}}{X_{CH4_{out}} + X_{CO} + X_{CO2} + 2X_{C2H4} + 2X_{C2H6}} \quad (3.2)$$

In above equation X stands for compositions and F stands for flow rates. Calculated output flow rate was then used to determine conversion and selectivity. Above equation were used rarely, because of the possibility of coke formation and heavy hydrocarbons formation at elevated temperatures.

Fourth and final choice was to use nitrogen as an internal standard in spite of associated problems; its peak was in the vicinity of oxygen peak and overlap problem happened in the case of large compositions for these gases. It took a huge amount of effort to find best conditions to get best separate peaks. Our previous experience had shown that generally higher methane to oxygen ratios were favored for OCM reaction [66, 67]. Therefore, oxygen composition was always less than 20 % and by taking a low composition for nitrogen, the way to use nitrogen as an internal standard was hampered. Nitrogen and oxygen peaks separation were good for column temperature less than 40 ˚C, but reaching such temperature was not practical for a GC instrument in room temperature and took a lot of time. So, an initial column temperature of 40 ˚C was chosen for a 5 minute period and then oven temperature increased with an increment rate of 20 ˚C min^{-1} to reach final temperature of 220 ˚C for 15 min, a bit less than maximum allowed temperature of column. A typical example of GC peaks and corresponding retention times is available in the Figure 3.2.

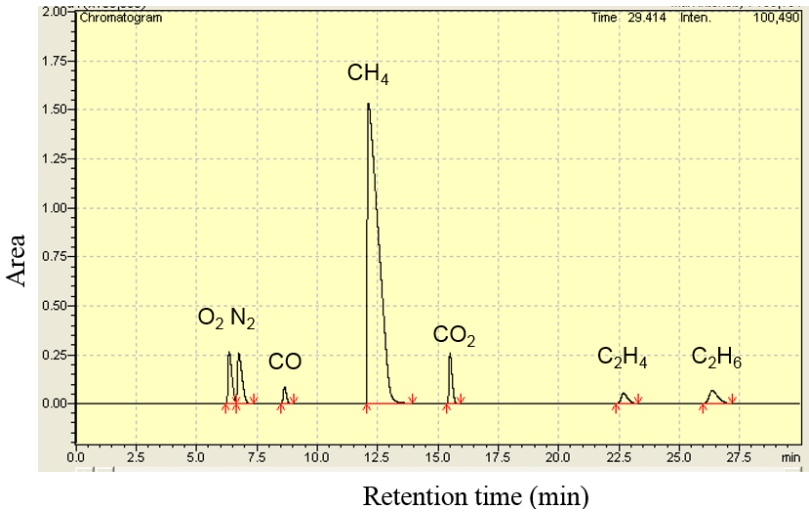

Figure 3.2. A typical example of GC output.

3.1.2. Mass Flow Controller

Specifications of two different types of MFC which were used in this study are listed in Table 3.2. These MFCs are calibrated using a soap bubble shown in the Figure 3.1. For calibration purpose, each gas was passed through individual MFC, which is set to the desired value, at least for 10 min. When the gas flow reached a stable condition, the time needed for replacement of bubble from a point to the other point which is precisely graded on bubble meter measured. This procedure is done six times for three different values (18 times in total for each set value) and an average value was calculated from these measurements and reported as the real value for set value. Real values versus set values were plotted and slope was calculated and used later to calculate set value for desired real values. MFC calibrations were done for all gases once, but for oxygen and nitrogen this calibration was done two times for two different regions. First calibration was for wide real values (20-80 ml min^{-1} for oxygen, 10-60 ml min^{-1} for nitrogen) and second calibration was for narrow real values (2-20 ml min^{-1} for oxygen, 2-10 ml min^{-1} for nitrogen). This is done because it was working at lower and higher concentrations of these gases. Furthermore, slight different behaviors for higher and lower compositions of nitrogen and oxygen were observed.

Table 3.2. MFC specifications.

Gas	Manufacturer	MFC Model
Inert He, N_2, O_2	OMEGA Engineering	FMA
GC He, CH_4	BROOKS Instrument	5850 E

3.1.3. Furnace, Furnace Controller and Thermocouple

A tubular electric furnace with a temperature range from 25-1000 ˚C and dimensions of 30 mm in diameter and 480 mm in length was used. Furnace was equipped with a FP-21 programmable controller, manufactured by Shimaden Corporation. Applied thermocouple was a K-type (Chromel (90% nickel and 10% chromium) Alumel (95% nickel, 2% manganese, 2% aluminum and 1% silicon)) which had a melting point of 1400 ˚C. This thermocouple attached to external part of the catalytic bed and inserted to the furnace along with the quartz reactor. Upper part of the furnace was always insulated using ceramic wool covered with aluminum foil, but lower part was not. This was done to have desired

temperatures at upper part of the reactor and lower temperatures at thinned part of the reactor which were located at lower part of the reactor.

3.1.4. Catalytic tests

Catalytic tests were carried out in a packed-bed, downward tubular reactor made of quartz. The reactor length was 800 mm with 10 mm inner diameter in the gas output and input part. Furthermore, reactor had a reduced diameter part with inner diameter of 2 mm, exactly after the catalyst bed. For each catalytic run, 200 mg particulate catalyst (30-80 mesh) or 2 monolith (each one containing 100 mg catalyst) were used. 200 mm of the upper, exactly before the catalytic bed, and 200 mm of the lower, exactly after the catalyst bed, part of the reactor was filled with quartz chips. For thicker part of the reactor, 1-2 mm quartz chips and for the reduced part, 0.63-1 mm quartz chips were used as filling material. Useless quartz glasses were crushed, sieved and washed by hydrochloric acid and acetone to produce desired quartz chips. Both monoliths and particulate catalyst were put on quartz wool and then covered again with small amount of quartz wool to make sure no contamination and mixing of quartz chips were taken place. A representation of this configuration is shown in Figure 3.3.

For each test, reactants (oxygen + methane = 96%) and internal standard (4% nitrogen) were mixed for 30 min using by-pass line and then analyzed using GC instrument. By-pass valve, oxygen and methane valve were closed. Using a three way valve, nitrogen was introduced to the reactor line while reaction line valve was open. Programmable temperature controller was started and desired program was loaded. For each experiment it took 50 min to reach set temperature; meanwhile nitrogen passes through the catalytic bed with a flow rate of 5 ml min^{-1} without reactants. 2 min before set temperature was reached, methane was introduced to the system and later oxygen was introduced. First data was taken after 20 min of reactants introduction. Every 50 min a datum was taken, this procedure continued for 370 min while the temperature remained constant.

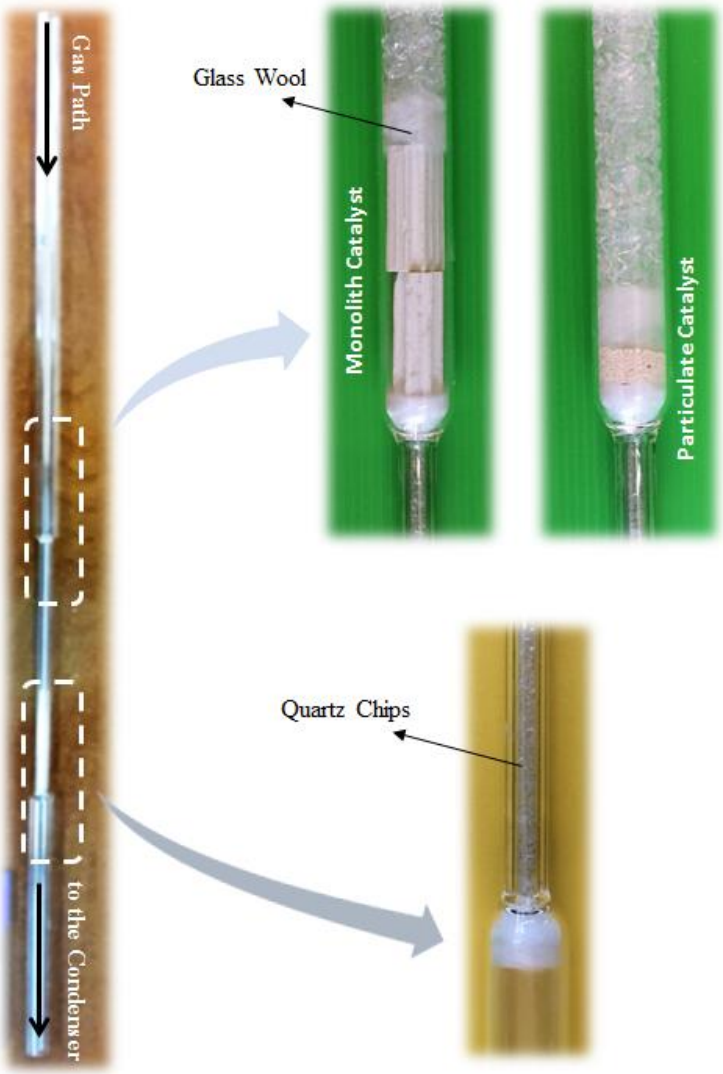

Figure 3.3. Quartz reactor and configuration of monolithic and particulate catalyst.

For the investigation of the temperature dependence, experiments with reaction temperature of 750, 800, 815, 825, 835, and 850 ˚C for particulate catalyst and 800, 835, 850 and 860 ˚C for monolith catalyst were conducted with a flow rate of 120 ml min^{-1}. Different CH_4/O_2 ratios were also tested to see the effect of this parameter on the activity and selectivity of the catalysts. Empty reactor and monolith catalyst filled with quartz chips (0.18-0.63 mm) also are tested and compared with other catalysts.

In all cases output flow rate was calculated using following Equation 3.3;

$$F_{Out} = \frac{X_{N2_{in}} \times F_{in}}{X_{N2_{out}}} \tag{3.3}$$

Following equations were used to calculate conversion, selectivity, and yield respectively (Equations 3.4-3.6);

$$Conversion = \frac{X_{CH4_{in}} \times F_{in} - X_{CH4_{out}} \times F_{out}}{X_{CH4_{in}} \times F_{in}} \quad (3.4)$$

$$Selectivity = \frac{2 \times F_{out}(X_{C2H4} + X_{C2H6})}{X_{CH4_{in}} \times F_{in} - X_{CH4_{out}} \times F_{out}} \quad (3.5)$$

$$Yield = Selectivity \times Conversion \quad (3.6)$$

3.2. Materials

3.2.1. Gases

A list of gases with detailed specifications used in this study and supplementary study is provided in Table 3.3.

Table 3.3. Gases used in this study and supplementary studies.

Gas	Formula	Specification	Type	Application
Helium	He	99.998%	Inert	GC Carrier Gas, reactor cooling gas
Methane	CH_4	99.995%	Reactant	GC calibration
Oxygen	O_2	99.999%	Reactant	GC calibration
Carbon Dioxide	CO_2	99.995%	Product	GC calibration
Carbon Monoxide	CO	99.5 %	Product	GC calibration
Ethylene	C_2H_4	5% C_2H_4 balanced with He	Product	GC calibration
Ethane	C_2H_6	5% C_2H_6 balanced with He	Product	GC calibration
Standard Mixture	CH_4, C_2H_6, C_2H_4	5% CH_4, 2% C_2H_6, 2% C_2H_4 balanced with He	Product	GC calibration
Nitrogen	N_2	99.998 %	Standard	Gas volume change indicator

3.2.2. Chemicals

Chemicals used in this study and supplementary studies are listed in Table 3.4.

Table 3.4. Chemicals used in this study and supplementary studies.

Chemicals	**Formula**	**Purity**	**Source**	**Size**	**Molecular weight**
Magnesium oxide	MgO	≥ 98%	Sigma-Aldrich	20-30 mesh	40.3 gr mol^{-1}
Magnesium oxide	MgO	≥ 98%	Sigma-Aldrich	30-80 mesh	40.3 gr mol^{-1}
Magnesium oxide	MgO	≥ 98%	Sigma-Aldrich	Less than 80mesh	40.3 gr mol^{-1}
Lithium nitrate	$LiNO_3$	≥ 98%	Fluka	Fine powder	68.9 gr mol^{-1}
Lithium acetate di-hydrate	$C_2H_3O_2Li.2H_2O$	Lithium acetate ≥63%	Sigma-Aldrich	Fine powder	102.0 gr mol^{-1}
Lanthanum (III) nitrate	$La(NO_3)_3.6H_2O$	≥ 99%	Merck	Fine powder	433.0 gr mol^{-1}
Strontium nitrate	$Sr(NO_3)_2$	≥ 99%	Merck	Fine powder	211.6 gr mol^{-1}
Silica Gel	SiO_2	≥ 99%	Sigma-Aldrich	60 - 100 mesh	60.1 gr mol^{-1}
Sodium tungstate di-hydrate	$Na_2WO_4.2H_2O$	≥ 99%	Sigma-Aldrich	Fine powder	329.9 gr mol^{-1}
Colloidal silica	SiO_2	≥ 99%	Sigma-Aldrich	40 wt.% aqueous Suspension	60.1 gr mol^{-1}
Manganese II nitrate tetra-hydrate	$Mn(NO_3)_2.4H_2O$	≥ 99%	Sigma-Aldrich	Fine powder	251.0 gr mol^{-1}
Quartz wool	SiO_2	≥ 99%	Leco	Fibrous	60.1 gr mol^{-1}

3.2.3. Catalyst preparation

3.2.3.1. Particulate catalyst preparation. Two methods were applied to prepare Li doped MgO catalyst; mixed mill and wet impregnation methods. Mixed mill method was

investigated because of its fastness and easiness to produce catalyst in large amounts which is of interest for industrial applications. Wet impregnation is the most common method applied to synthesize Li/MgO catalyst for OCM reaction.

In mixed mill method, MgO (smaller particles than 80 mesh) were milled in a ceramic mortar and pestle. Milled MgO were sieved and particles less than 0.18 mm (80 mesh) were mixed and milled with appropriate amounts of lithium acetate dihydrate ($CH_3COOLi.2H_2O$ water content 37 wt.%) using mortar and pestle to produce 0.5 wt.% Li/MgO. Afterward the prepared samples were calcined at 400˚C for 3h. This procedure was done also for $LiNO_3$ as another precursor for Li.

In wet impregnation method, MgO particles (between 30-80mesh) were weighted and mixed with appropriate amount of lithium ethanoate ($CH_3COOLi.2H_2O$) to produce 0.5 wt.% Li/MgO and dissolved in just sufficient deionized water to form a thick paste. After 30 min of thoroughly mixing, prepared paste was dried at 120 ˚C for 4h and calcined at 750 ˚C for 6h.

3.2.3.2. Monolith catalyst preparation. Commercial mullite monolith shown in Figure 3.4 (Kale Porselen, Mullite C530) were cut into the dimensions of 17 mm × 8 mm × 9 mm in order to place it easily in 10 mm ID quartz reactor. Final shape of each monolith had 16 square channels with dimensions of 1 mm × 1mm × 17 mm and average weight of 0.88 gr. After cutting into desired dimensions, shaped monoliths were washed with acetone to remove probable contaminations during cutting procedure and then dried in oven.

MgO were milled in mortar and pestle. Milled MgO were sieved and particles smaller than 0.18 mm (80mesh) were suspended in appropriate amount of deionized water (0.5 ml for each monolith) while mixing with ultrasonic mixer. Shaped monoliths were dipped and rolled inside the slurry while mixing with an ultrasonic mixer. Every 5 min excess MgO which was clogging the openings were flushed out by pressurized air and with the help of a needle. After 30 min of mixing and rolling inside slurry, monoliths were dried for 40 min inside a microwave oven. Using this method resulted in at least 0.15 gr MgO coated monolith. Subsequently excess MgO were scrubbed using a needle and by tapping each monolith to the table surface. This procedure is done several times to reduce the amount of

coated MgO to 0.1 gr per monolith and separate weak adhered MgO particles from the monolith surface.

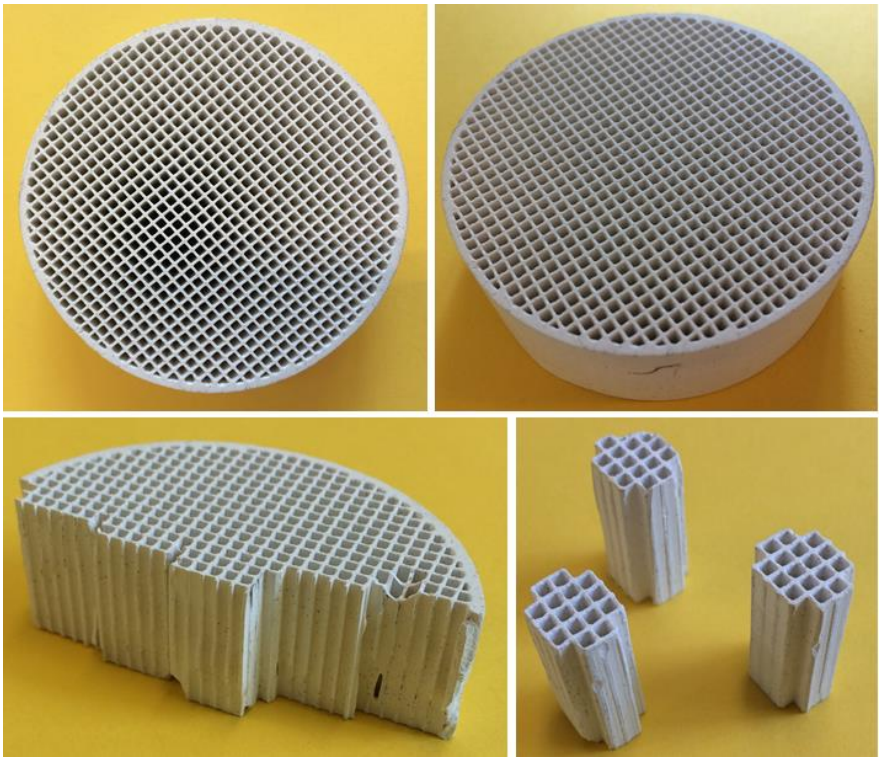

Figure 3.4. Mullite monolith used in this study.

When 0.1 gr of MgO was coupled on each monolith successfully, appropriate amount of $CH_3COOLi.2H_2O$ is dissolved in 0.2 ml of deionized water per monolith (0.5 wt.% Li/MgO) for 15 min assisted with ultrasonic mixer. Active metal solution then was injected using a syringe thoroughly and drop by drop to the channels of each monolith one by one. When all channels were full of droplets, theses droplets were pushed forward by slow blowing inside channels. External surface of the monoliths were wetted by droplets as well as internal surface. Afterward the prepared sample was dried at 120 ˚C for 4 h and calcined at 750 ˚C for 6 h. Schematic of this procedure is illustrated in Figure 3.5.

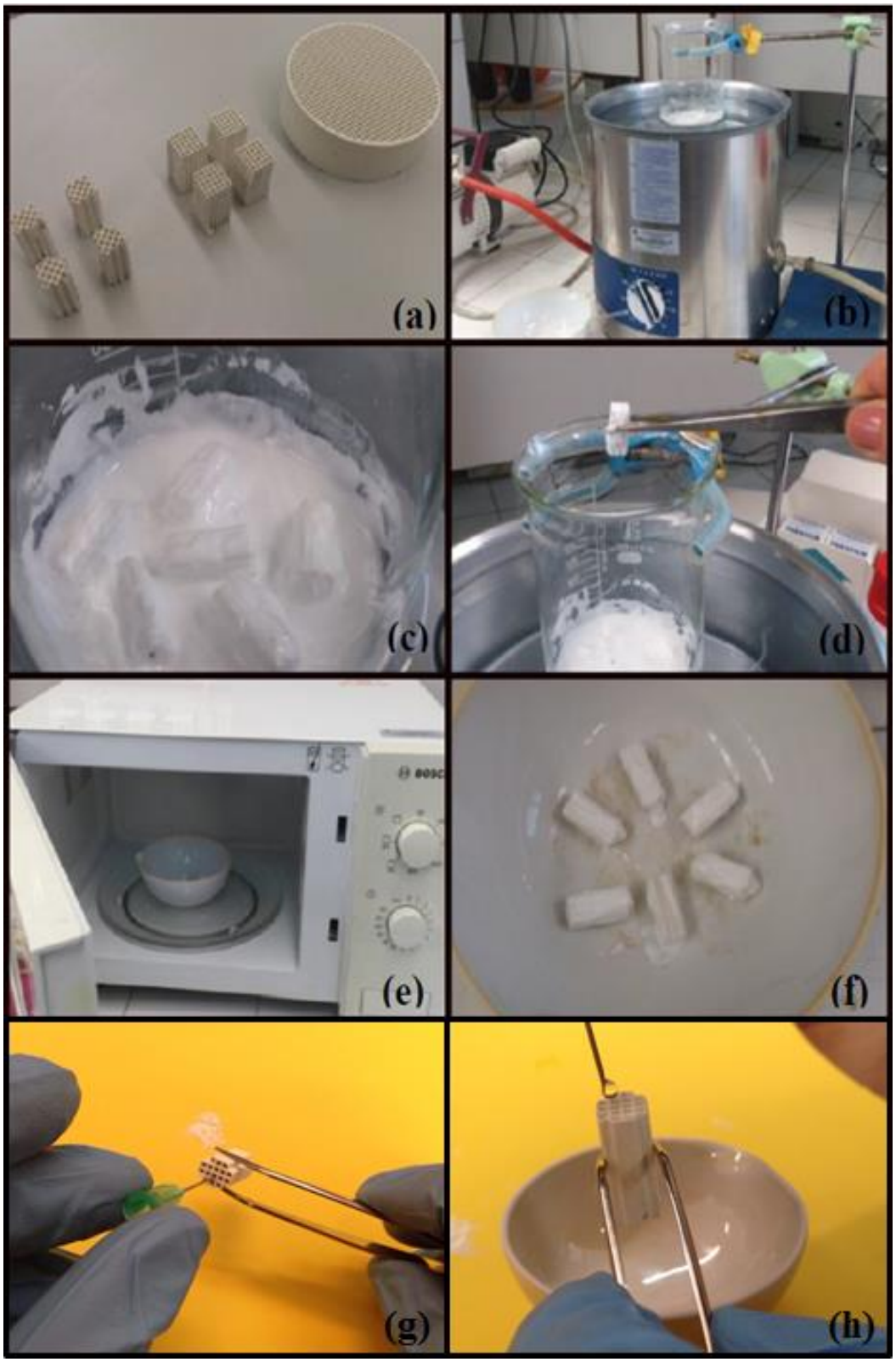

Figure 3.5. Monolith coating procedure; (a) Shaping the Monolith to Suitable Size, (b) Preparing suspension of magnesium oxide, (c) dipping procedure in ultrasonic mixer, (d) compressed air flow, (e) drying at microwave oven, (f) MgO coated monoliths, (g) excess MgO scrubbing, (h) Li injection.

4. RESULTS AND DISCUSSION

4.1. Performance Tests

Particulate and monolith catalyst have been tested under same conditions; total flow of 120 ml min^{-1} was used over 200 mg of 0.5 wt.% Li/MgO catalyst. An 800 mm quartz reactor with id of 10 mm, which was reduced to 2 mm after first 400 mm of the reactor (just after the catalyst bed) was used. This reactor shape was used because previous experiments (on the same system) of Dusova [66] and Sezen [67] had shown that better performance was observed if the internal diameter of the reactor was reduced. Idea of fast evacuating product gases from the system also is proposed by many researchers [6, 7, 45].

4.1.1. Particulate Catalyst

4.1.1.1. Effect of Li Precursor. Two different precursors of Li ($LiNO_3$ and $CH_3COOLi.2H_2O$) which have been widely used in previous studies for 0.5 wt. % Li/MgO catalyst were tested using mixed mill method. Particles smaller than 80 mesh were tested in four different temperatures (see Figure 4.1).

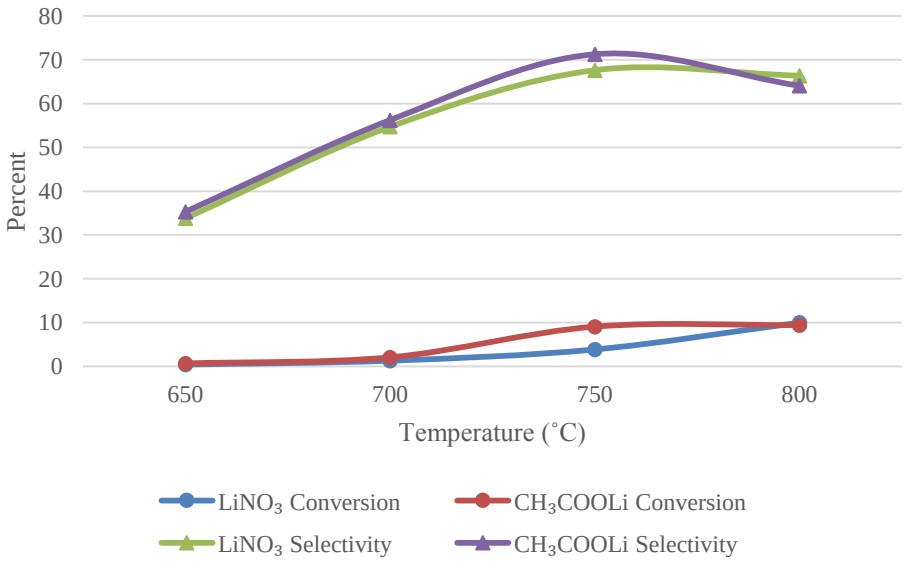

Figure 4.1. Precursor effect on particulate catalyst at CH_4/O_2=7.

CH_3COOLi derived catalyst showed slightly better performance than $LiNO_3$ derived alternatives at least at 750 ˚C, even though the conversion was still low for both cases; the conversion values for $LiNO_3$ derived catalyst and for CH_3COOLi derived catalysts were 3.9 and 9.1 respectively. Based on this experiment CH_3COOLi was selected as precursor of Li for other experiments.

4.1.1.1. Effect of Operational Variables. Effect of temperatures was also investigated for particulate catalyst. Reactor was heated for 50 min in 5 ml min^{-1} of pure nitrogen to reach desired temperature. Then, methane was introduced to the reactor followed by oxygen. First data was taken 20 min after introduction of reactants. Every 50 min, a new datum was taken; 8 data points were taken during 370 min of activity test and plotted versus time.

Figure 4.2 represents activity tests for 0.5 wt.% Li/MgO particulate catalyst at various temperatures and CH_4/O_2 = 7. In all cases 0.2 gr catalyst was used with a total flow of 120 ml min^{-1}. For CH_4/O_2=7, the best operating temperature was 815 ˚C, which resulted in a conversion of 20 % and yield value of 8%.

In all figures in the next page, except for highest and lowest temperature, there is an activity decrease for particulate catalyst as time elapses. This can be explained by the loss of active metal (Li) through the time. As time passes, lithium content of catalyst decreases while LiOH and Li_2SO_3 is produced (see Figure 2.3) as also suggested by Korf *et al.* and Kasteren *et al.* [30, 56]. Activity decrease continues until the Li content of the catalyst reaches its solubility in MgO lattice which is 0.01-0.03 wt. % based on Arndt [7].

For all cases, a disturbance was observed for the first data which was taken after 20 min of reaction started; this was not consistent with the trend line drawn for other data points. This disturbance can be explained by poor mixing and heating of reactants within 20 min after the reactants were introduced. On the other hand, OCM reaction is highly exothermic and the instability within the first 20 min could be also partially explained by the time required to reach a thermal equilibrium for gases and catalyst.

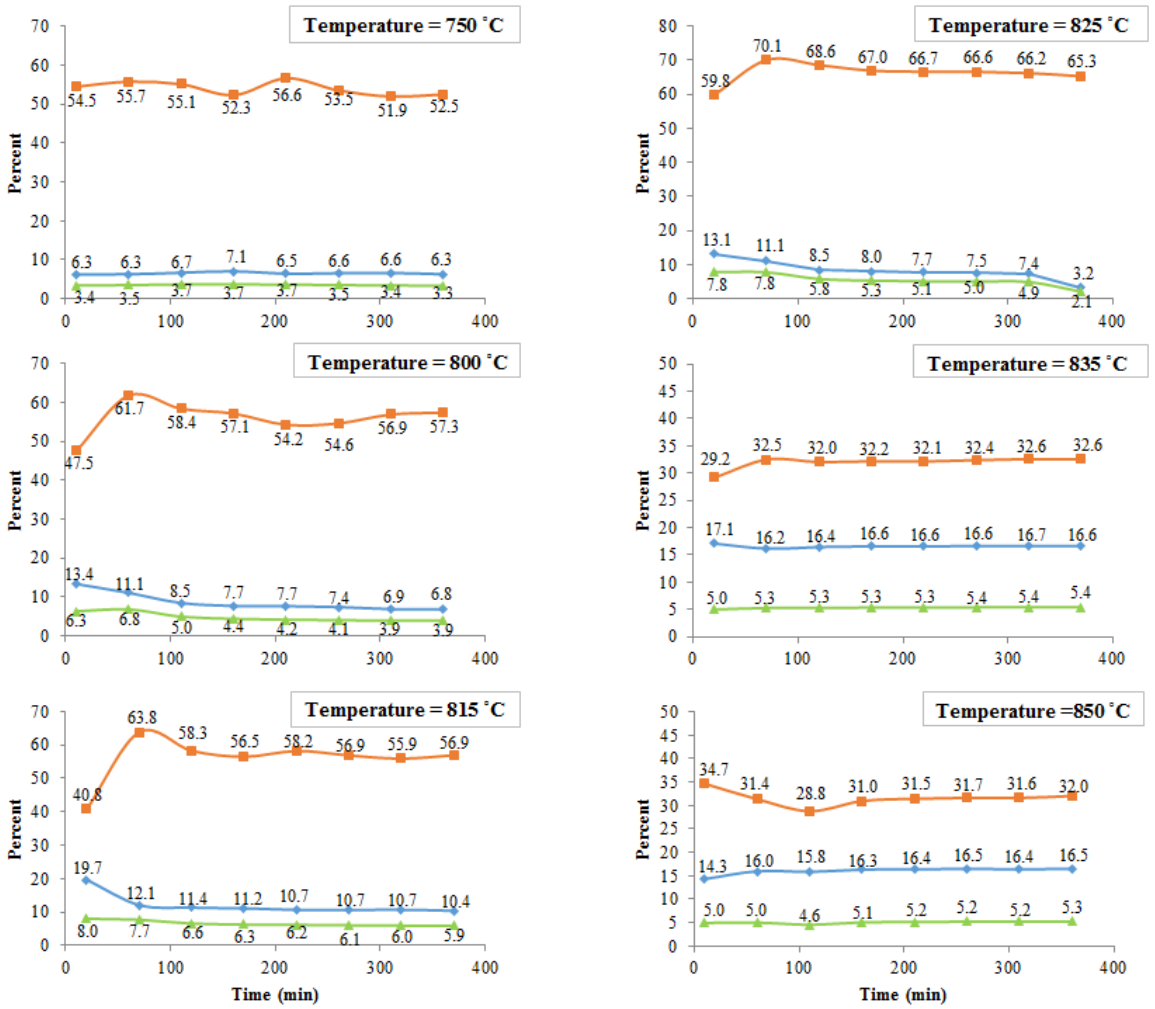

Figure 4.2. Activity tests for particulate catalyst at CH_4/O_2=7.

It is believed that, at lower and higher temperatures, this catalyst is not active, and the activities observed at these temperatures are independent from the type or even the presence of catalyst; this value could be obtained even in empty reactor. Constant conversion, selectivity and yield over time support this theory for 750, 835, and 850 ˚C. Figure 4.3 compares performance of empty reactor with the one containing catalyst; in both cases CH_4/O_2 is 7. It is obvious that catalyst loses its activity within first hours of reaction, which can be attributed to loss of lithium at elevated temperatures. Selectivity and conversion of the catalyst reaches a constant and seemingly stable value, which is a bit higher than value for empty reactor. This low activity can be attributed to low lithium residual remained in the catalyst which is not volatile and is trapped in the lattice of MgO.

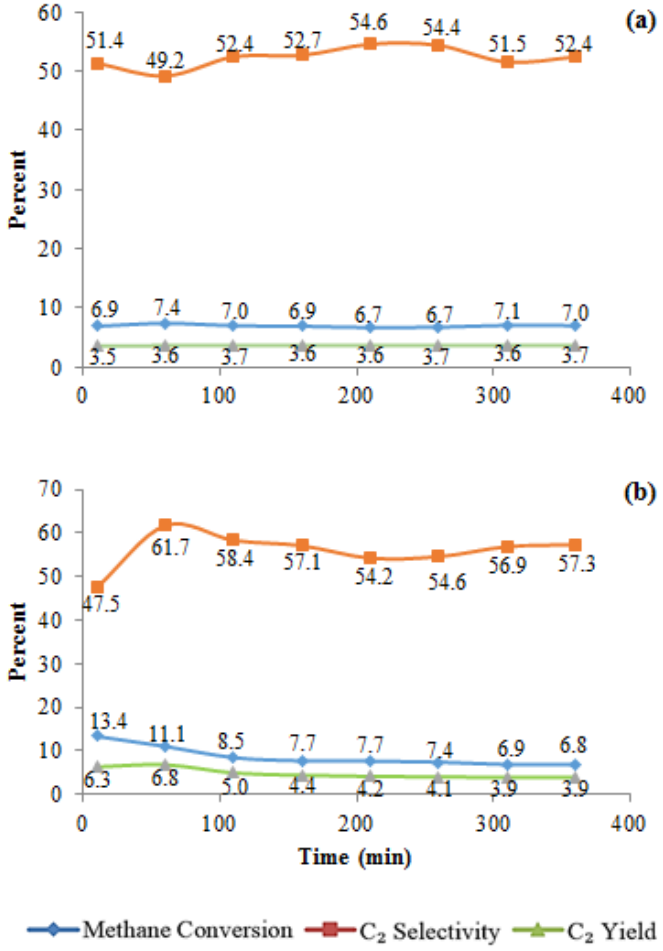

Figure 4.3. Activity comparison of (a) empty reactor and (b) particulate catalyst at 800˚C and methane to oxygen ratio of 7.

Based on all experiments, a general rule can be deduced: the selectivity is low when the conversion is high, and vice versa. Although this behavior is obvious almost in all experiments, and is more apparent at first data points where the conditions are not stable. The reaction starts with a high conversion value while selectivity is low, after a while selectivity increases while conversion decreases.

Different methane to oxygen ratios are also investigated for particulate catalyst. Figure 4.4 represents this investigation at 815 ˚C after 20, 120, 220, and 320 min of the reaction. It is obvious that lower methane to oxygen ratios are more favorable for OCM conversion over 0.5 wt.% Li/MgO particulate catalyst. However, generally higher selectivities for C_2 hydrocarbons was observed for higher CH_4/O_2 but the net effect of methane oxygen ratio on

C_2 yield was negative. It seems that higher CH_4/O_2 also favors the oxidation path of methane and as a result decreases the C_2 hydrocarbons production.

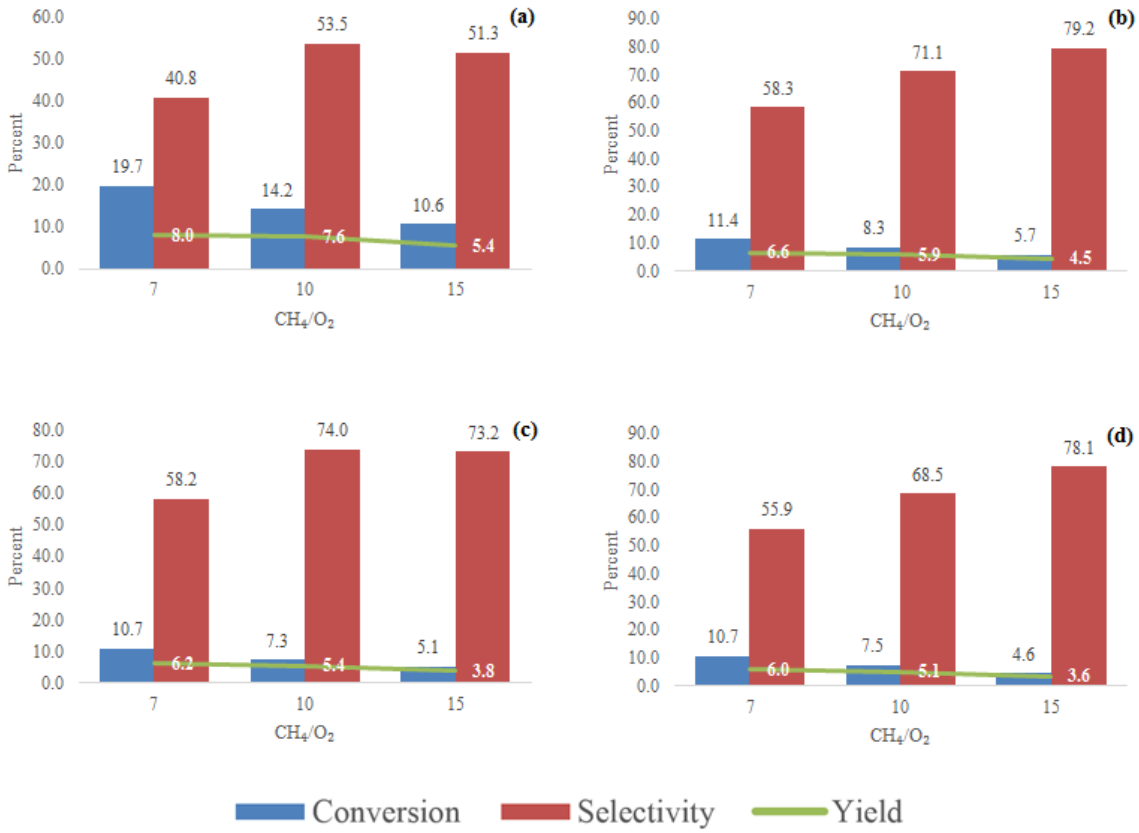

Figure 4.4. CH_4/O_2 effect on particulate catalyst at 815 ˚C after (a) 20 min (b) 120 min (c) 220 min (320) min.

4.1.2. Monolith Catalyst

Mullite monolith, which was cut and shaped to be placed in a 10 mm id quartz reactor was coated with 0.2 gr of 0.5 wt.% Li/MgO catalyst using dip-coating method. Afterward, this catalyst was tested under the same conditions of particulate catalyst tests (i.e. total flow of 120 ml min^{-1} and a GHSV of 36000 cm^3 gr^{-1} h^{-1}). Activity testes were carried out for two monoliths (each monolith approximately 8.5 mm OD, 20 mm length and contained 0.1 gr of catalyst), which were placed in a reduced id quartz reactor. Thermocouple was adjusted exactly between two monoliths to make sure an average temperature of two monoliths was reached. Figure 4.5 provides the results of activity tests done on monolithic structure.

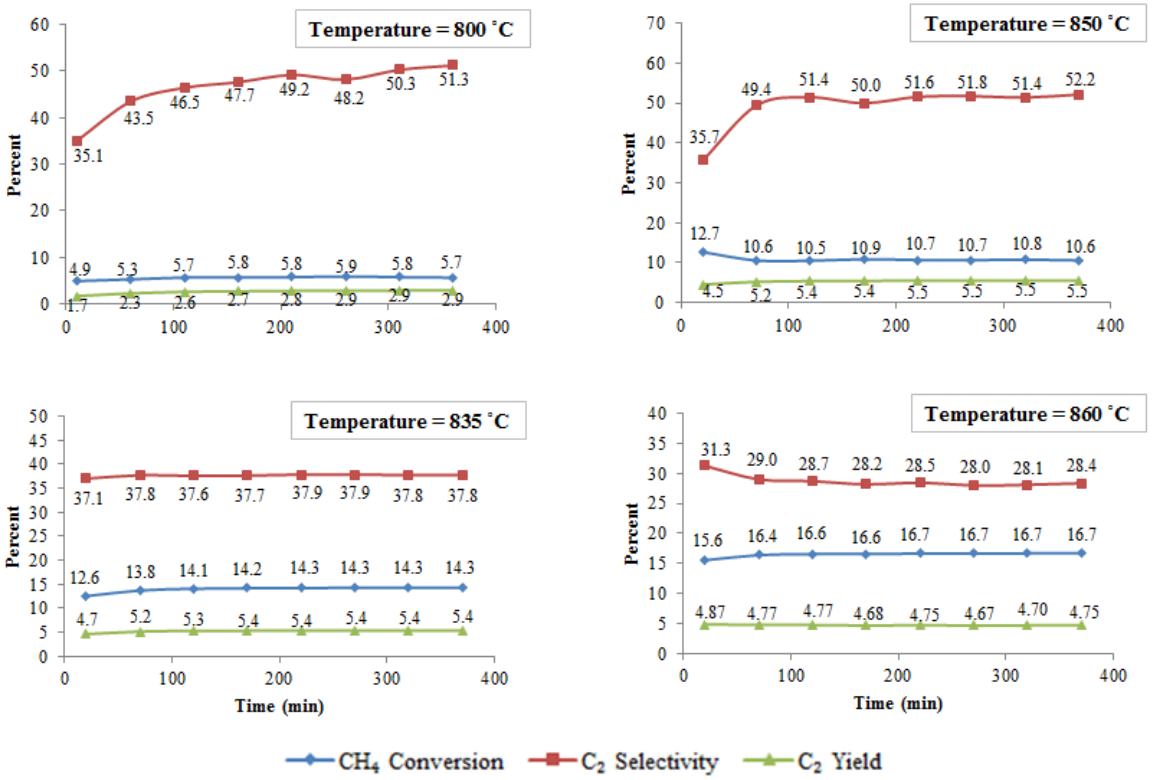

Figure 4.5. Activity tests for mullite monolith catalyst at CH_4/O_2=7.

Interestingly, as Figure 4.5 shows, monolith catalyst activity increased slightly by time unlike particulate catalyst, which showed declining activity through the time. This behavior can be explained by the time, which is needed for monolith catalyst to reach a thermal equilibrium with reactant gases after introduction. Same disturbance for the first data, which is taken 20 min after reaction start, was also observed. Like particulate catalyst this disturbance is thought to be related to the exothermicity of the reaction and poor mixing of product gases after 20 min of reaction initiation, which is not enough to reach a thermal equilibrium.

For almost, all cases, monolith catalyst showed poorer performance than particulate catalyst; this performance was even worse than empty reactor at 800 ˚C. It is believed that monolith works like a cold spot for OCM reaction and by this way decreased its activity. As time elapsed, the monolith activity increased; this shows that monolith catalyst was getting warm and reaching a thermal equilibrium with reactants. On the other hand, it is obvious that monolith structure suffers extremely from heat transfer problem. To solve this drawback a solution is proposed in recommendation section of this study.

CH_4/O_2 effect was also investigated for monolithic structure and illustrated in Figure 4.6. Same as particulate catalyst, the lower methane to oxygen ratios are more favorable for C_2 yield; at higher values of CH_4/O_2, reactions that are favored are the complete or partial oxidation of methane.

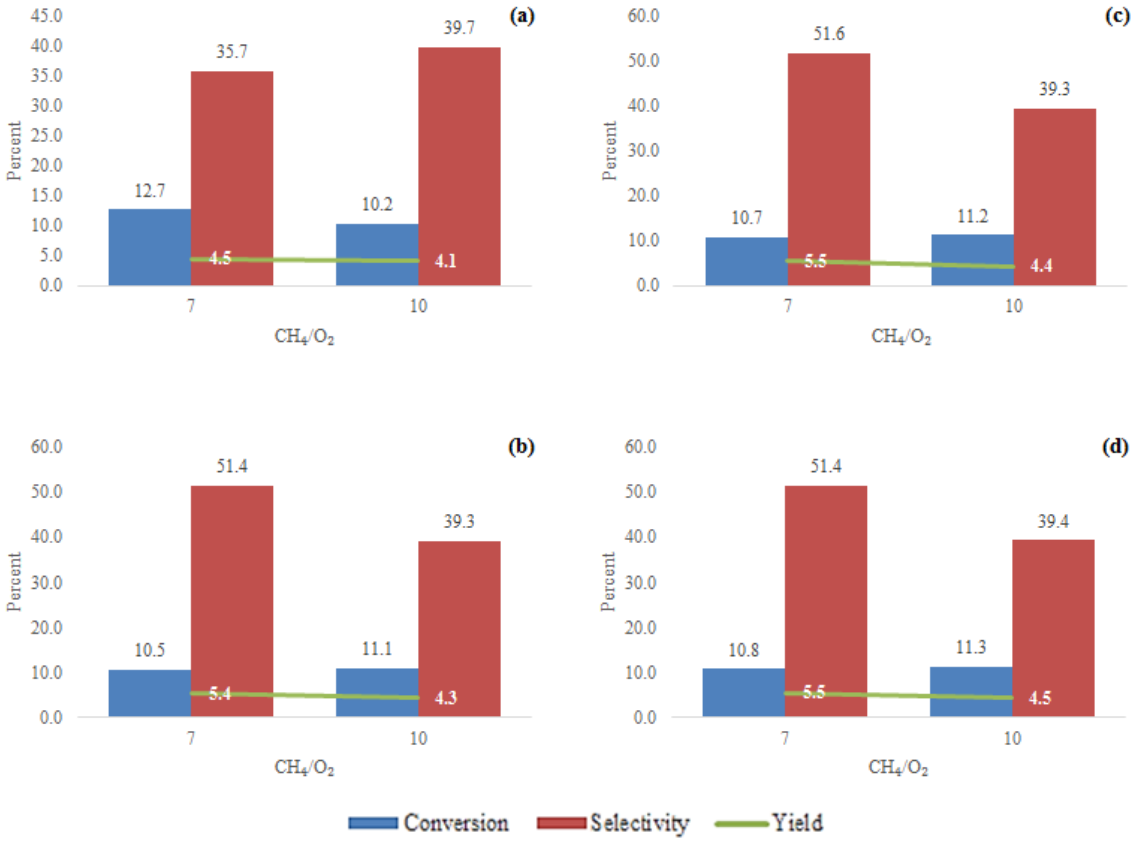

Figure 4.6. CH_4/O_2 effect on Monolith catalyst at 850 ˚C after (a) 20 min (b) 120 min (c) 220 min (320) min.

Lithium doping was one of the biggest problems, which came across for monolithic structure. Generally in wet impregnation method, the lithium ions can freely move and have enough time to accommodate themselves in MgO structure for particulate catalysts whereas it was not possible for Li containing droplets to penetrate through the coated layer of MgO on cordierite monolith. On the other hand, dipping of monolith in lithium dissolved solution was not applicable because it was possible to lose a portion of magnesium oxide in the active metal loading step. Therefore, it would not be possible to report the weight percent of active metal loaded on monolith.

Beside above mentioned tests, the heat transfer improvement of monolithic structure was also investigated by adding quartz chips (0.18-0.63 mm) inside the channels of catalyst coated monolithic structure. This experiment was done at 850 ˚C, at which the monolith catalyst showed its best performance (see Figure 4.7), with the hope that the heat transfer could be improved. As Figure 4.7 shows, the methane conversion was slightly increased at all temperature tested. But at the same time, C_2 hydrocarbons selectivity was decreased, and as a result, the net yield of monolith was unchanged.

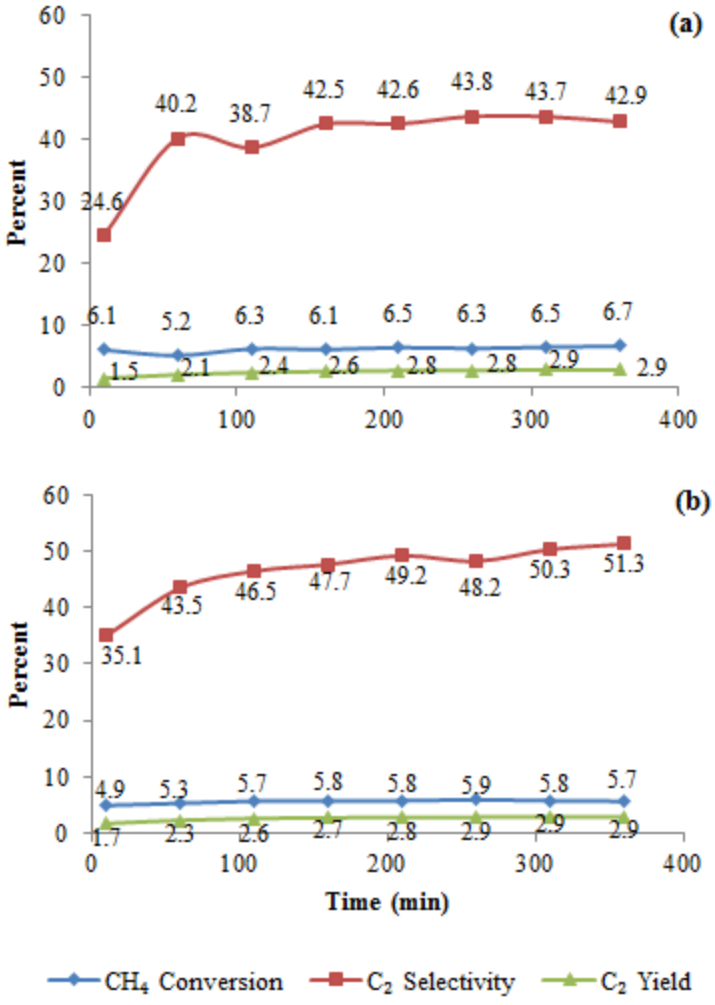

Figure 4.7. Catalyst performance at 800 ˚C and CH_4/O_2 = 7 for (a) filled monolith with quartz chips (b) empty monolith.

4.1.3. Summary

A comparison between the performance of the particulate and monolith catalyst against temperature is provided in Figure 4.8. These data are taken within first 20 min of the reaction initiation for both monolith and particulate catalyst. It is believed that stable activity of the monolith catalyst is not related to the monolithic structure and this activity would be obtained even if the catalyst did not exist. Higher temperatures for monolith catalyst and lower temperature for particulate catalyst were tested because monolithic structure showed better performance at elevated temperatures.

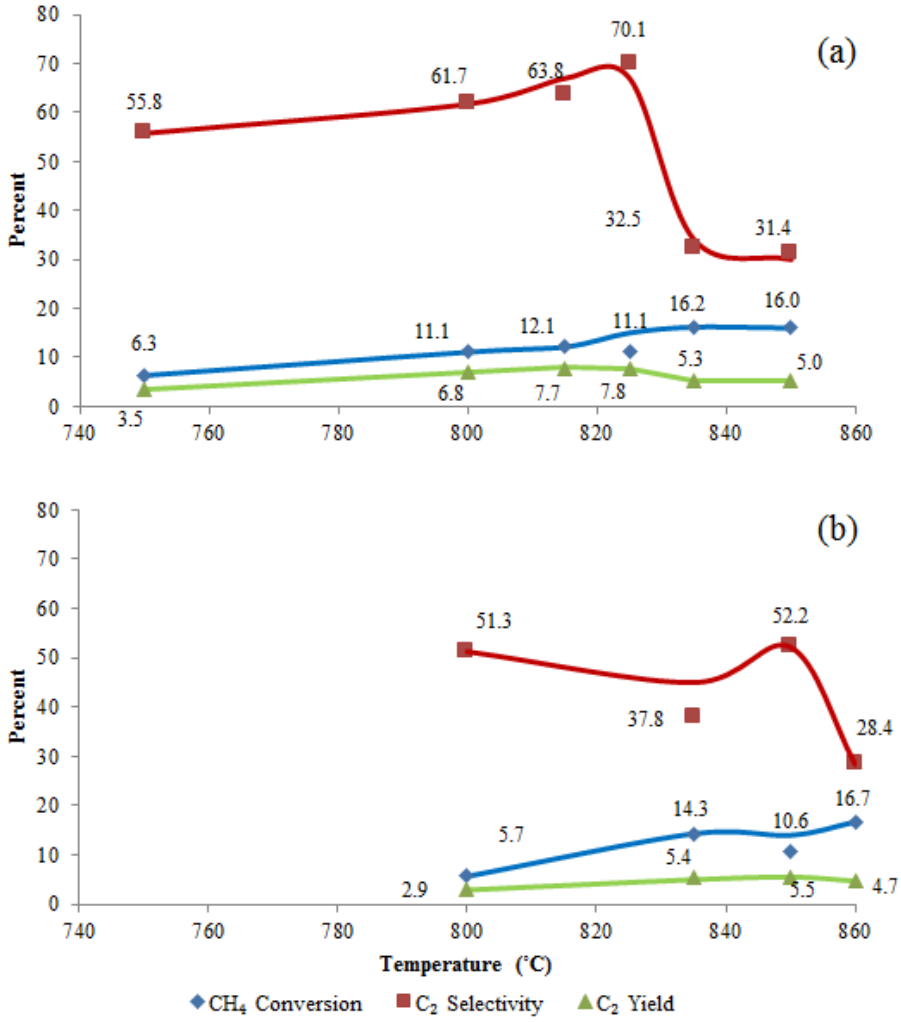

Figure 4.8. (a) Particulate catalyst vs. (b) monolith catalyst at CH_4/O_2=7.

Methane conversion for both particulate and monolith catalyst increased by increasing temperature. C_2 hydrocarbons selectivity increase was also observed by elevating

temperature but after an optimum point a sharp decline was observed for both catalyst structures. This optimum point was 815 ˚C and 850 ˚C for particulate catalyst and monolith catalyst, respectively.

4.2. Catalyst Characterization

The crystalline phases of the catalyst samples and their particle sizes were identified by using a Rigaku D/MAX-Ultima+/PC X-Ray diffraction equipment having an X-ray generator with Cu target. Micrographs of the fresh and used catalyst samples as well as the support materials were also taken using an environmental scanning electronic microscope (ESEM), to observe the morphological differences. X-ray analytical mapping and Energy Dispersive X-Ray Spectroscopy (EDX) tests were also conducted on catalyst samples in order to clarify their elemental analysis and to obtain information on the dispersion and stability of the metals on the catalyst surface. The tests were conducted in a Philips XL 30 ESEM-FEG system, having a maximum resolution of 2 nm. The experiments were performed at the Advanced Technologies Research and Development Center of Boğaziçi University.

4.2.1. SEM and EDX

Lithium was among three light elements that could not be detected by EDX. The energy reflected by light elements is so small that a big portion of it can be scattered by the air particles before reaching the detector. Usually, to improve the detection of light elements, X-Ray impact process is implemented at vacuum conditions. But, even at extreme vacuum condition, the detection of very light elements may not be possible, and lithium is among them. Furthermore, it must be noted that EDX composition analysis given by the instrument is valid only for specific area that is specified by the operator and cannot be considered as a total measurement of the catalyst.

Fortunately, using two different detectors mounted on the ESEM apparatus a shadow difference between light and heavy elements was possible to see. Using these feature lithium loss was observed. Figure 4.9 represents SEM images of 0.5 wt.% Li/MgO particulate catalyst before and after reaction. Using EDX instrument it was verified that shinning clusters in (b) and (e) images of the Figure 4.9 were CaO, which can be explained by

impurities came from MgO support; these clusters are shown with yellow arrows. On the other hand, shinning dots, which are different in color and size (see Figure 4.9.c) from CaO are possibly Li particles. These dots are faded in images which are taken after reaction (see of Figure 4.9.f); these dots are shown with red arrows.

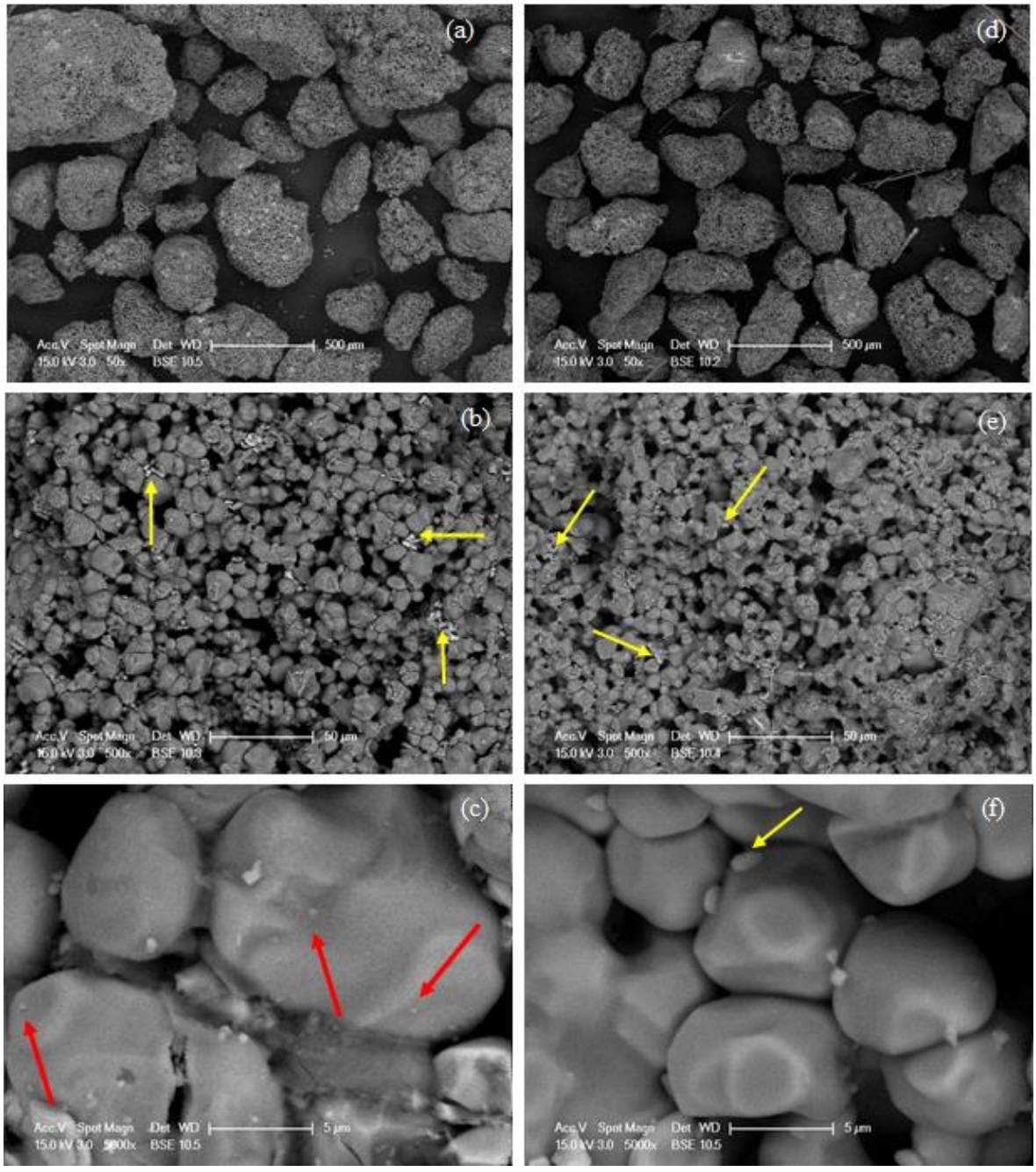

Figure 4.9. SEM images of 0.5 Li/MgO particulate catalyst (a), (b), and (c): before reaction; (d), (e), and (f): after reaction, yellow arrows represent CaO cluster while red ones probably are Li particles.

Coating support using dip-coating method for mullite monolith does not seem a well suited technique because support formed a layer on the edges of square channels and the other parts of the monolithic structure had bare areas. This can be easily seen in Figure 4.10, which was taken from a monolith cut vertically after dip-coating. Dark areas are well coated areas while bright areas were not well during dip-coating procedure.

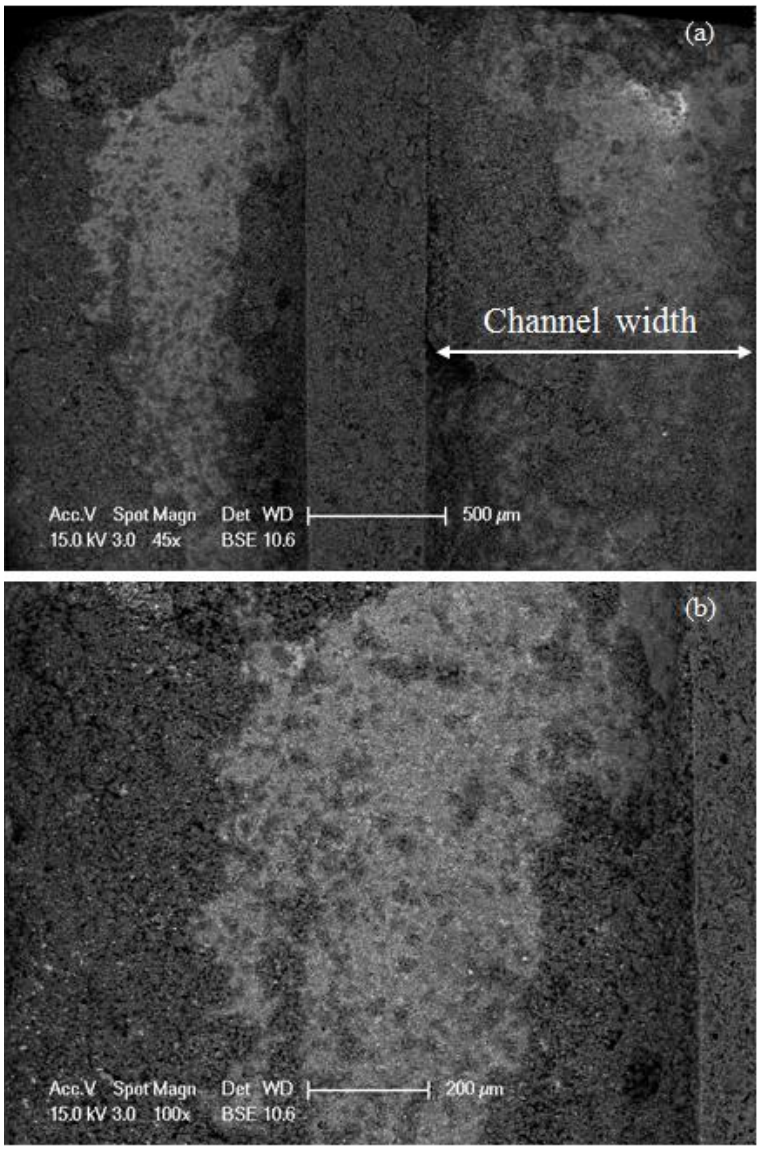

Figure 4.10. Horizontal view of cut monolith after dip-coating procedure.

4.2.2. XRD

Figure 4.11 represents XRD result of 0.5 wt.% Li/MgO particulate catalyst which matched with MgO peaks. Li peaks were not expected to be seen because of lightness of this

element but the peak indicated by red squares in Figure 4.11 may possible be Li peak, which is faded in the XRD results of catalyst after reaction (see Figure 4.11.b).

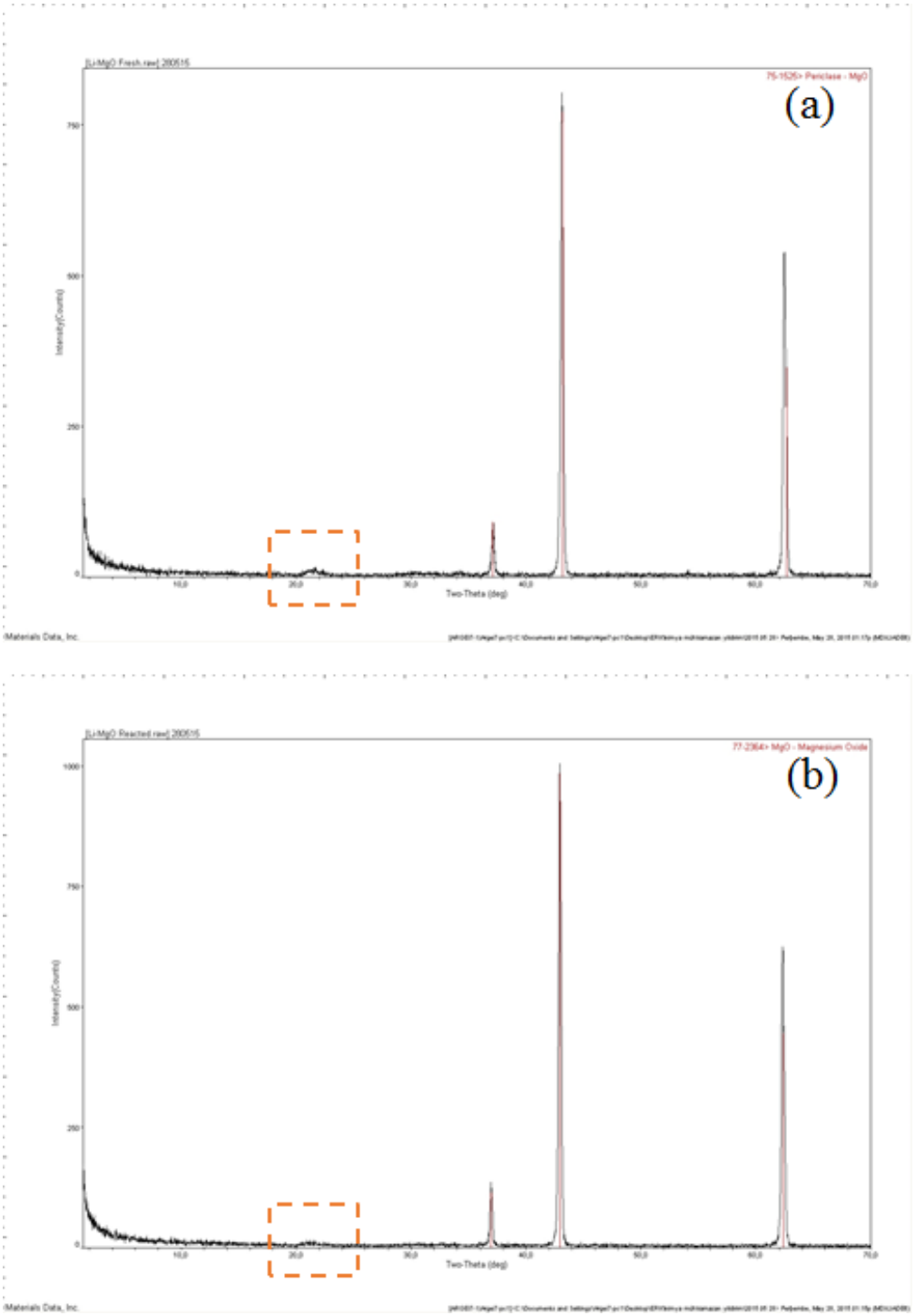

Figure 4.11. XRD results of 0.5 wt.% particulate catalyst (a) before reaction and (b) after reaction.

5. CONCLUSION

0.5 wt. % Li/MgO particulate catalyst prepared using mixed mill and wet impregnation method and dip-coating monolith catalyst were investigated for OCM reaction. All catalytic tests were done in a reduced id quartz reactor exactly after catalyst bed and at a GHSV of 36000 cm^3 gr^{-1} h^{-1} with 0.2 gr of catalyst. To sum up following points were concluded.

(i) OCM is a homogenous-heterogeneous reaction; to decrease gas phase reactions, which favors CO_x production, the product gases must be evacuated and quenched from the reaction environment as soon as possible. For this purpose, reactor diameter decrease exactly after catalytic bed seems practical solution.

(ii) Li/MgO catalyst is not stable; it loses its Li content within the first hours of reaction. This behavior was observed for all catalysts tested. It is believed that Li reacts with OH^- anion and produce LiOH which is volatile.

(iii) Quartz reactor is not suitable reactor for OCM reaction over Li/MgO catalyst because present Li in the catalyst reacts with quartz and produces Li_2SO_3.

(iv) Li based catalysts are not proposed for further investigations for OCM reaction; because OCM reaction takes place at elevated temperatures which Li is not stable.

(v) Mullite monolith seems to suffer from heat transfer problem. Therefore, this structure is not suitable for OCM reaction, which is highly exothermic and needs a catalyst structure with supreme heat transfer. Further investigations must be done to improve heat transfer of this structure before its wide applications. An innovative heat transfer improvement was proposed at recommendation part of this study.

(vi) CH_4/O_2 ratio must be optimized; so high or so low values decrease activity. For this study a value of 7 showed slightly better performance than higher values.

(vii) As time elapses in OCM, reaction shifts toward production of ethylene rather than ethane.

(viii) Monolithic structure needs higher temperatures to get active. Optimum activity was seen at 850 ˚C for monolithic structure while this value for particulate catalyst was 815 ˚C.

6. RECOMMENDATIONS

Following points are recommended to improve monolithic structure not only for OCM reaction but also for other reactions, which take place at high temperatures and need high mechanical stability. Nano-wire catalyst in a modified micro-channel reactor and metal framework reinforced monolith heated using an induction furnace are completely new ideas which are proposed for the first time in this study.

6.1. General Points

- Lithium can be added to the MgO slurry (in appropriate amount) directly in the MgO coating step and then coat on the monolithic structure. Using this method will minimize poor distribution of lithium on the monolith surface in the syringe injection method.
- Ceramic reactor or silicon carbide reactor are highly recommended to be tested for Li/MgO catalyst. One of the biggest drawbacks of quartz reactor was its reaction with lithium to produce Li_2SO_3. Therefore, application of quartz reactor is not recommended. High thermal conductivity, low thermal expansion, and high corrosion resistance of SiC makes it a promising reactor material candidate for severe exothermic and endothermic reactions.
- OCM is introduced as a heterogeneous-homogenous reaction which happens at solid and gas phase [7]. It is recommended to design a reactor with a thinned part exactly after the catalyst bed which is equipped with a quench device to minimize gas phase reactions.

6.2. Experimental setup design

Applied system in this study had some drawbacks which made it hard to work with it and caused some limitations to experiments. Some of these disadvantages are listed below.

- Only one reactor mounted in one furnace was used, so only one experiment per day was done.

- Furnace was in tubular form and because of it, reactor must be mounted from the upper part. This caused some troubles for reactor mounting and some of reactors were broken or cracked during mounting procedure. Furthermore, thermocouple adjustment was hard because the catalytic bed was located at the center of the furnace and was not easily reachable.
- Measured temperature by thermocouple was indicating the temperature of external wall of quartz reactor. This temperature is not a good indicator of catalytic bed. Imbedded thermocouple in catalytic bed must be used.

All above mentioned problems could be solved using a well-designed catalytic test setup. Such a setup is shown in Figures 6.1 and 6.2; this setup was used by Arndt *et al.* to investigate stability of Li/MgO catalyst [7]. As following figures illustrate there are 6 individual furnaces equipped with reactors, MFCs, gages, condensers, and controllers which are compressed in a transportable chamber (see Figure 6.1). On the other hand, Figure 6.2 shows a typical furnace which can be opened from the front side. This feature will omit need to mount reactor from the top of the furnace and will ease thermocouple adjustment.

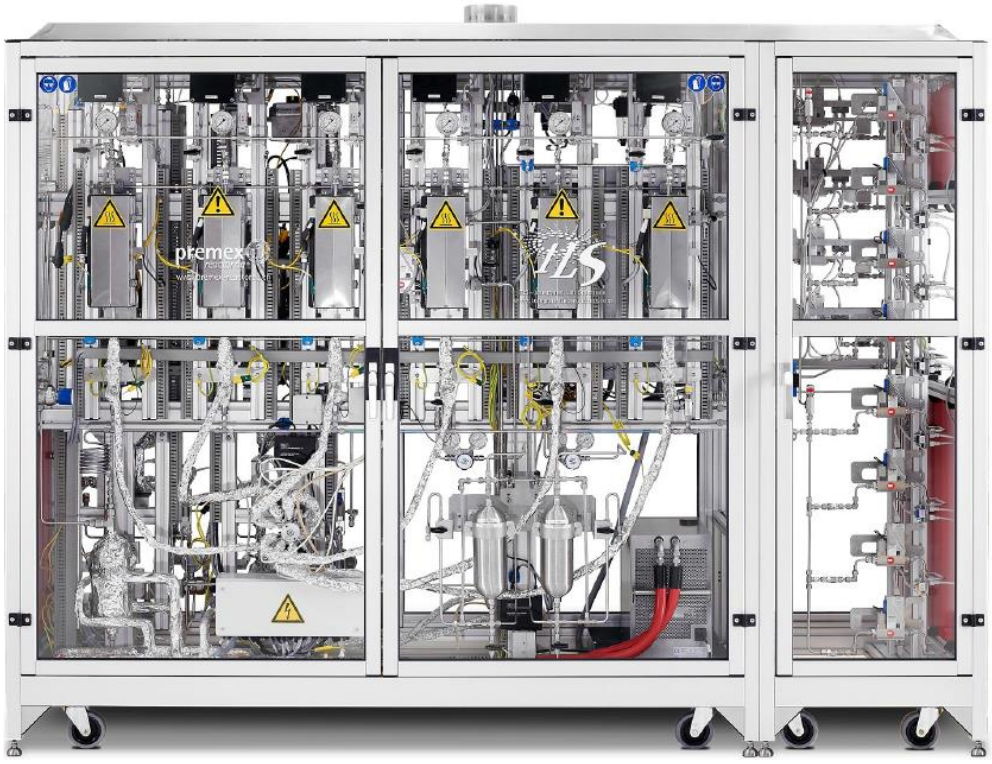

Figure 6.1. Front view of proposed configuration for experimental system [7].

Figure 6.2. Close view of proposed configuration for experimental setup [7].

6.3. Nanowire catalyst in a modified micro-channel reactor

One of the innovative configurations which is going to be discussed in this study for the first time for future studies is nanowire catalyst in a modified micro-channel reactor. But some key technologies must be explained before explanation of proposed configuration.

What is going to be discussed is only a brief introduction on some technologies, which are applied in proposed configuration.

6.3.1. Nanowire Technology

Nanomaterials have gained a lot of interest due to their supreme performance in optics, electronics, photo-catalysis, and photonics. One-dimensional nano-structures such as nanowires, nano-rods (short nanowires), nano-fibers, nano-belts, and nanotubes have been used in both research and industrial applications [68].

ZnO nanowires grown on flexible poly-L-lactide nano-fibers are used as photo-catalyst for water purification. The continuous flow photo-catalytic decomposition of organic compounds in water has no need for separation of photo-chemically active material from the reservoir, and the purified water can be directly collected from reservoir [69]. Figure 6.3 shows aligned ZnO nano-rods grown on a cylindrical shape substrate [70].

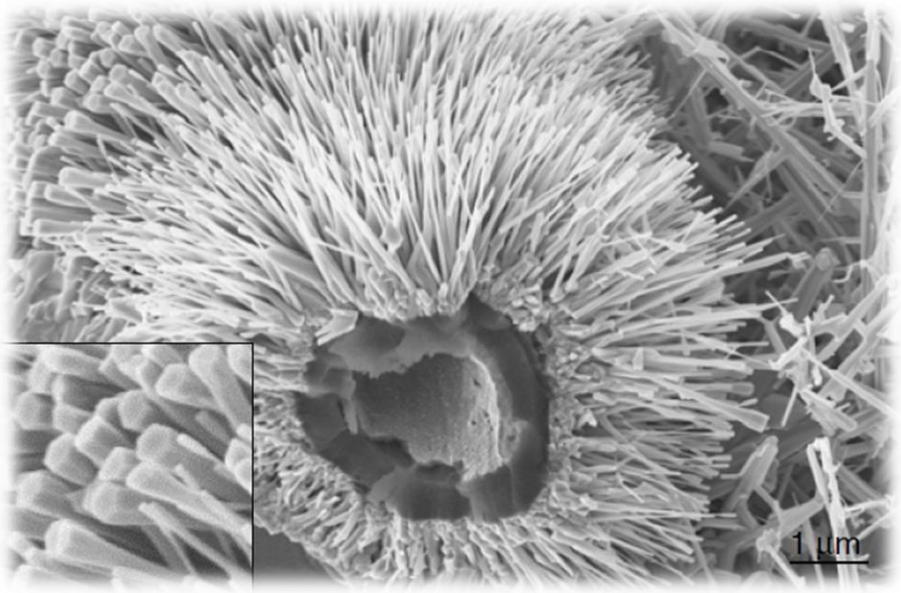

Figure 6.3. ZnO nano-rods grown on a cylindrical substrate. Reprinted with permission from [70] via Copyright Clearance Center.

Nanowire nickel catalyst is used in partial oxidation of methane to syngas. Results were literally promising. A comparison of metallic nickel and nanowire catalyst is provided

in Figure 6.4. BET surface area showed a 0.25 m^2 gr^{-1} for metallic Ni catalyst while this value for nanowire nickel catalyst was 9.77 m^2 gr^{-1}[71].

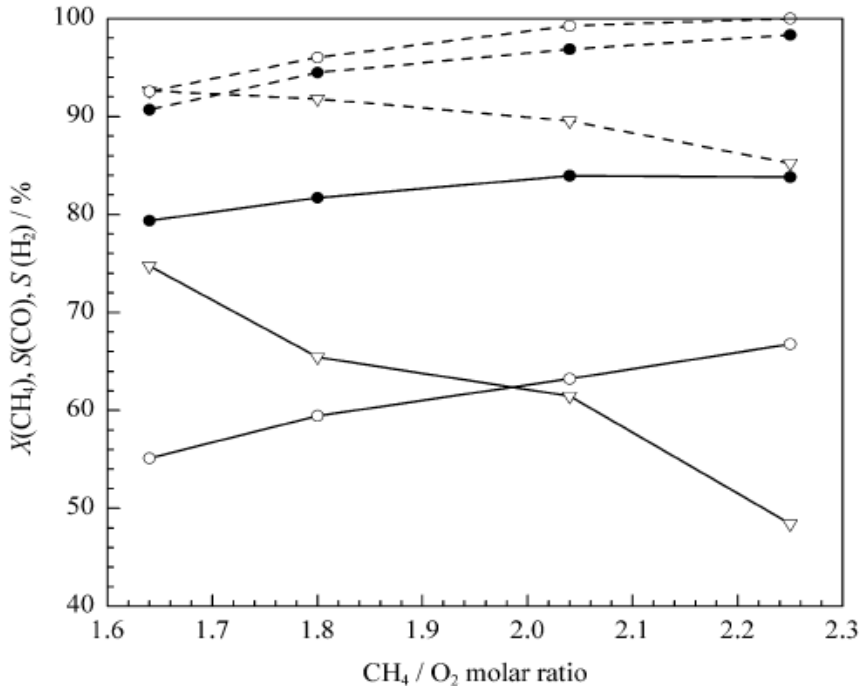

Figure 6.4. Comparison of CH_4 conversions and H_2 and CO selectivities between metallic Ni catalyst (solid lines) and the nickel nanowire catalyst (dashed lines) at different CH_4/O_2 ratios. (▽) methane conversion, (○) H_2 selectivity, (●) CO selectivity. Reaction conditions= 850°C, GHSV= 2.0×104 h^{-1}. Reprinted with permission from [71] via Copyright Clearance Center.

6.3.2. Flame Spray Technology

Thermal spraying techniques are coating processes in which melted (or heated) materials are sprayed onto a surface. The feedstock (coating precursor) is heated by electrical (plasma or arc) or chemical means (combustion flame). Thermal spraying can provide thick coatings (approx. thickness range is 20 µm to several mm, depending on the process and feedstock), over a large area at high deposition rate as compared to other coating processes. Coating materials available for thermal spraying include metals, ceramics and composites. They are fed in powder or wire form, heated to molten or semi molten state and accelerated towards substrate in the form of micrometer-size particles. Combustion or electrical arc discharge is usually used as the source of energy for thermal spraying [72]. A summary of

this technology is represented in Figure 6.5. This technology can be used to coat powdered materials like MgO, ZnO, Al_2O_3, and so on.

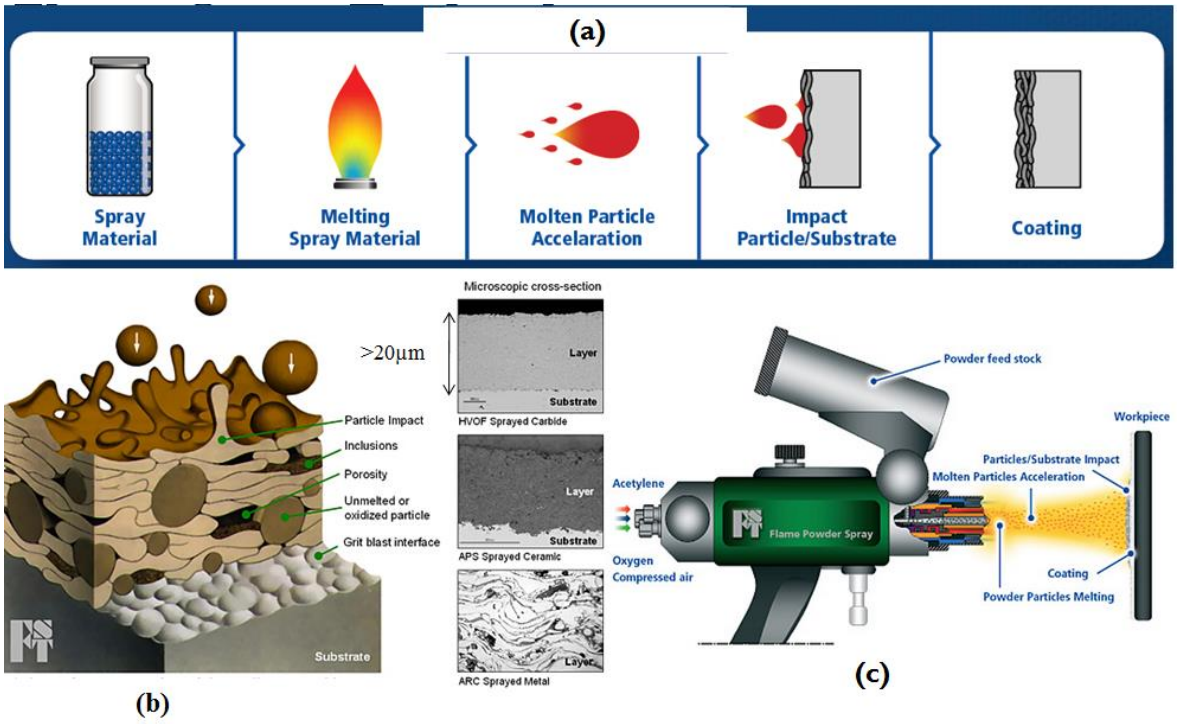

Figure 6.5. Summary of FSP technology (a) thermal spray process (b) cross-section of thermal sprayed layer (c) flame powder spraying gun [72].

6.3.3. Micro-channel reactor

Micro-channel reactor is considered as an advantageous technique for highly exothermic and endothermic reactions because of improved heat transfer characteristics. Usually, blade coating method is used to coat a layer of catalyst on a thin plate and then this plate is inserted to the micro-channel reactor. Adhesion problem of many catalyst to this blade results in application limitation for this technology. Dusova tried to coat 2wt.% Mn / 5wt.% Na_2WO_4 / SiO_2 over a FeCrAl plate to use it in micro-channel reactor for OCM reaction but it was unsuccessful because of poor adhesion of catalyst to the plate [66]. It is proposed in this study to coat catalyst to the blade of micro-channel reactor with flame spray technology which has supreme adhesion.

6.3.4. Proposed Configuration

Combination of nanowire technology with flame spray technology and micro-channel reactor which is made of silicon carbide for OCM reaction is illustrated in Figure 6.6. This innovative configuration is proposed for first time in this thesis.

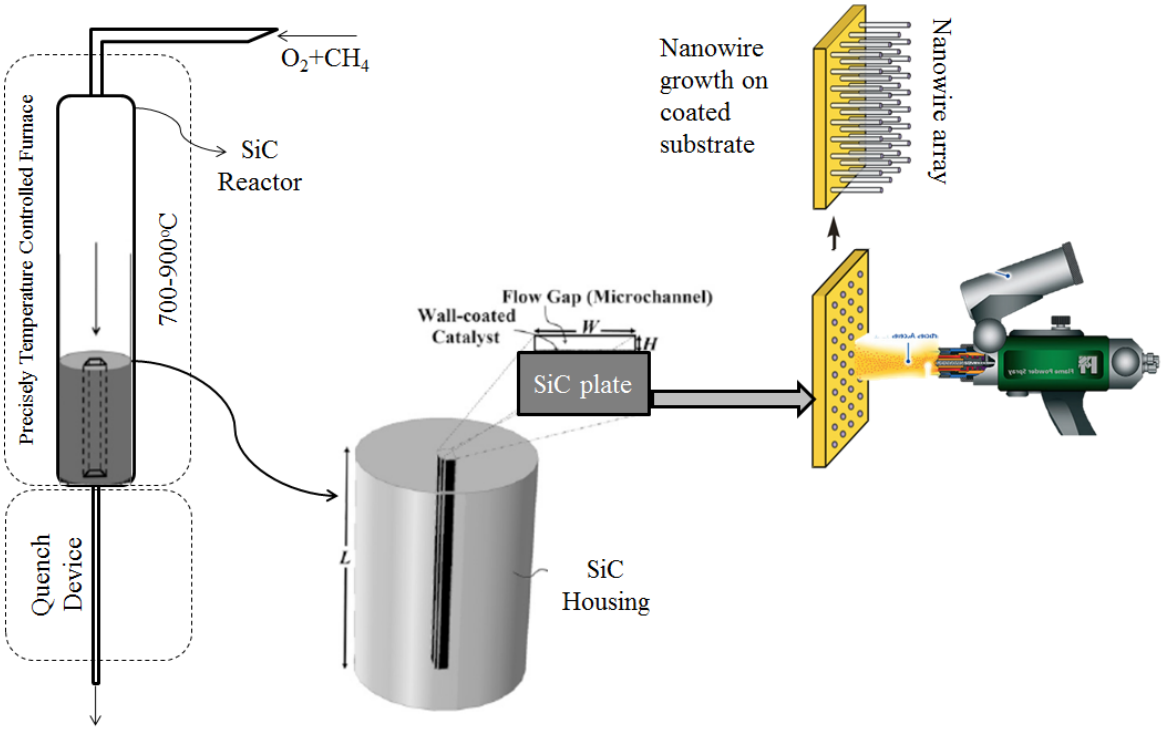

Figure 6.6. Proposed configuration for OCM reaction in a nanowire catalyst in modified micro-channel reactor.

In Figure 6.6 micro-channel reactor is used because of its supreme heat transfer specification and suitability for high exothermic and endothermic reactions which is critical for OCM reaction. Nanowire catalyst used because it provides extremely high surface area as well as pure surface area -in comparison with particulate catalyst- for highly exothermic reaction of OCM. Flame spray technology is used because it is believed that this method will give a tremendous adhesion to the catalyst and will increase stability of nanowires at high temperatures of OCM reaction.

6.4. Heat Transfer Improvement of Monolithic Structure

An innovative heat transfer improvement for monolithic structure (monolith and monosil) is proposed in this study for the first time. But before explanation of method, fundamentals must be explained.

6.4.1. Induction Heating Theory

Michael Faraday was the first person who discovered induction heating in 1831. Faraday's law of induction states that "the electro-motive force (emf) induced in a circuit is directly proportional to the time rate of change of magnetic flux through the circuit. An alternating voltage applied to an induction coil will result in an alternating current in the coil circuit. An alternating coil current will produce in its surroundings a time variable magnetic field that has the same frequency as the coil current. This magnetic field induces eddy currents in the work piece located inside the coil. Eddy currents will also be induced in other electrically conductive objects that are located near coil. These induced currents have the same frequency as the coil current; however, their direction is opposite to the coil current. These currents produce heat by the Joule effect (I^2R). A conventional induction heating system that consist of a cylindrical load surrounded by a multi-turn induction coil is shown in Figure 6.7 [73].

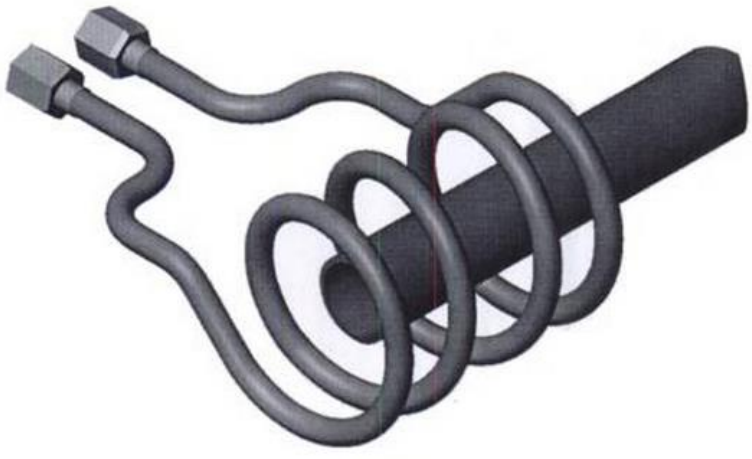

Figure 6.7. Conventional induction heating system consists of a cylindrical load surrounded by a multi-turn induction coil [73].

6.4.2. Proposed Induction Heating Improved Monolithic Structure

Monolithic structures mainly are made of ceramic materials; therefore it is not possible to induce current in the monolithic structure in order to produce heat. But if monolithic structure had a metal framework inside, it would be possible to induce heat on the metallic framework and consequently produce heat inside the monolithic structure without any contact. This metal frame work can be imbedded inside monolith structure at production step or at gelation step for monosil structure. To imagine this configuration, see Figure 6.8. In this configuration needles represents metal framework and pink cylinder represents monolithic structure which is placed inside a quartz reactor. Heat induced using coil around the quartz reactor in metal framework and hereby heated whole of the monolith in once. It must be noted that this figure is only to give an imagination of what is proposed and is not a practical setup.

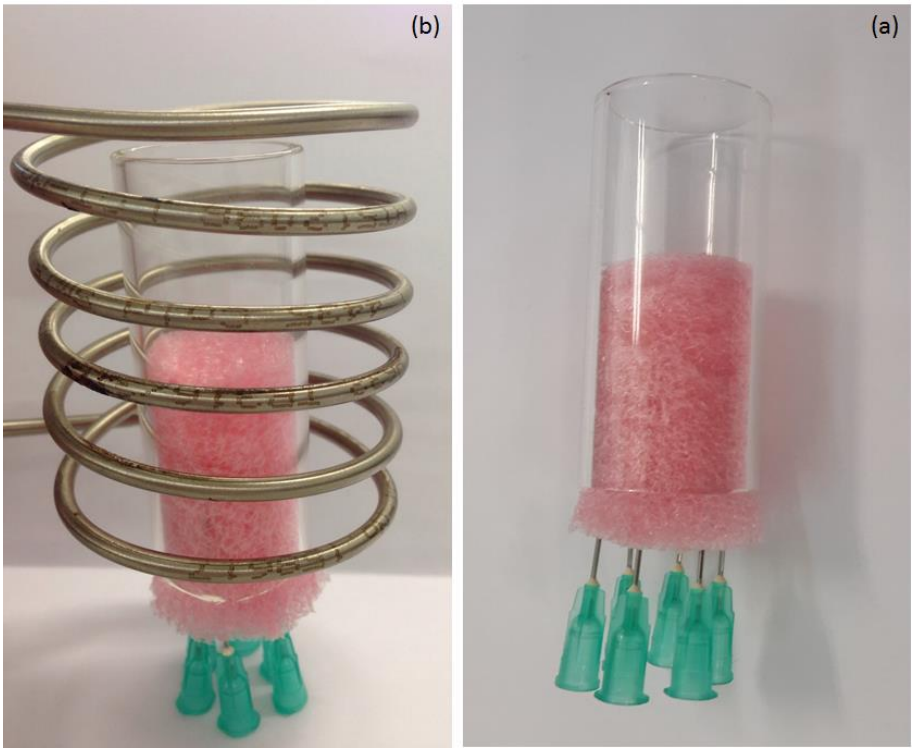

Figure 6.8. Schematic of proposed configuration for induction heating of monolithic structure (a) metal framework without coil (b) metal framework with heating coil.

REFERENCES

1. Langfeld, K., *Impact of Synthesis Methods and Oxidizing Agents on the Catalytic Performance of Various Catalysts in the Oxidative Coupling of Methane,* M.S. Thesis, Technical University of Berlin, 2012.

2. B.P., *Bp Statistical Review of World Energy,* 64th edition, B.P., London, 2015.

3. Lunsford, J. H., "The Catalytic Oxidative Coupling of Methane", *Angewandte Chemie International Edition in English*, Vol. 34, No. 9, pp. 970-980, 1995.

4. Ito, T., J. Wang, C. H. Lin, and J. H. Lunsford, "Oxidative Dimerization of Methane over a Lithium-Promoted Magnesium Oxide Catalyst", *Journal of the American Chemical Society*, Vol. 107, No. 18, pp. 5062-5068, 1985.

5. Holmen, A., "Direct Conversion of Methane to Fuels and Chemicals", *Catalysis Today*, Vol. 142, No. 1–2, pp. 2-8, 2009.

6. Zavyalova, U., M. Holena, R. Schlögl, and M. Baerns, "Statistical Analysis of Past Catalytic Data on Oxidative Methane Coupling for New Insights into the Composition of High-Performance Catalysts", *ChemCatChem*, Vol. 3, No. 12, pp. 1935-1947, 2011.

7. Arndt, S., *Stability of Lithium Doped Magnesium Oxide and Zinc Oxide Catalysts for the Conversion of Natural Gas,* Ph.D. Thesis, Technical University of Berlin, 2010.

8. Mleczko, L. and M. Baerns, "Catalytic Oxidative Coupling of Methane—Reaction Engineering Aspects and Process Schemes", *Fuel Processing Technology*, Vol. 42, No. 2–3, pp. 217-248, 1995.

9. Amenomiya, Y., V. I. Birss, M. Goledzinowski, J. Galuszka, and A. R. Sanger, "Conversion of Methane by Oxidative Coupling", *Catalysis Reviews*, Vol. 32, No. 3, pp. 163-227, 1990.

10. Kondratenko, E. V. and M. Baerns, "Oxidative Coupling of Methane", *Handbook of Heterogeneous Catalysis*, pp. 3010, 2008.

11. Lunsford, J. H., "Catalytic Conversion of Methane to More Useful Chemicals and Fuels: A Challenge for the 21st Century", *Catalysis Today*, Vol. 63, No. 2-4, pp. 165-174, 2000.

12. Arndt, S., G. Laugel, S. Levchenko, R. Horn, M. Baerns, M. Scheffler, R. Schlögl, and R. Schomäcker, "A Critical Assessment of Li/MgO-Based Catalysts for the Oxidative Coupling of Methane", *Catalysis Reviews*, Vol. 53, No. 4, pp. 424-514, 2011.

13. Choudhary, V. R., S. A. R. Mulla, M. Y. Pandit, S. T. Chaudhari, and V. H. Rane, "Influence of Precursors of Li2o and MgO on Surface and Catalytic Properties of Li-Promoted MgO in Oxidative Coupling of Methane", *Journal of Chemical Technology & Biotechnology*, Vol. 75, No. 9, pp. 828-834, 2000.

14. Matsuura, I., Y. Utsumi, T. Doi, and Y. Yoshida, "Oxidative Coupling of Methane over Lithium-Doped Ultrafine Crystalline Magnesium Oxide", *Applied Catalysis*, Vol. 47, No. 2, pp. 299-306, 1989.

15. Arndt, S., U. Simon, S. Heitz, A. Berthold, B. Beck, O. Görke, J. D. Epping, T. Otremba, Y. Aksu, E. Irran, G. Laugel, M. Driess, H. Schubert, and R. Schomäcker, "Li-Doped MgO from Different Preparative Routes for the Oxidative Coupling of Methane", *Topics in Catalysis*, Vol. 54, No. 16-18, pp. 1266-1285, 2011.

16. Lopez, T., I. Garcia-Cruz, and R. Gomez, "Synthesis of Magnesium Oxide by the Sol-Gel Method: Effect of the Ph on the Surface Hydroxylation", *Journal of Catalysis*, Vol. 127, No. 1, pp. 75-85, 1991.

17. López, T., R. Gómez, A. Ramírez-Solis, E. Poulain, and O. Novaro, "Li/MgO Sol-Gel Catalysts", *Journal of Molecular Catalysis*, Vol. 88, No. 1, pp. 71-84, 1994.

18. Trionfetti, C., I. V. Babich, K. Seshan, and L. Lefferts, "Efficient Catalysts for Olefins from Alkanes: Sol–Gel Synthesis of High Surface Area Nano Scale Mixed Oxide Clusters", *Topics in Catalysis*, Vol. 39, No. 3-4, pp. 191-198, 2006.

19. Choudhary, V. R., S. A. R. Mulla, and B. S. Uphade, "Influence of Support on Surface Basicity and Catalytic Activity in Oxidative Coupling of Methane of Li–MgO Deposited on Different Commercial Catalyst Carriers", *Journal of Chemical Technology & Biotechnology*, Vol. 72, No. 2, pp. 99-104, 1998.

20. Berger, T., J. Schuh, M. Sterrer, O. Diwald, and E. Knözinger, "Lithium Ion Induced Surface Reactivity Changes on MgO Nanoparticles", *Journal of Catalysis*, Vol. 247, No. 1, pp. 61-67, 2007.

21. Zavyalova, U., M. Geske, R. Horn, G. Weinberg, W. Frandsen, M. Schuster, and R. Schlögl, "Morphology and Microstructure of Li/MgO Catalysts for the Oxidative Coupling of Methane", *ChemCatChem*, Vol. 3, No. 6, pp. 949-959, 2011.

22. Taniewski, M., A. Lachowicz, and K. Skutil, "Effective Utilisation of the Catalyst Bed Deactivating in the Course of Oxidative Coupling of Methane", *Chemical Engineering Science*, Vol. 52, No. 6, pp. 935-939, 1997.

23. Kuo, Y., F. Behrendt, and M. Lerch, "Effect of the Specific Surface Area of Li/MgO Catalysts in the Oxidative Coupling of Methane", *Zeitschrift für Physikalische Chemie*, Vol. 221, No. 8, pp. 1017-1037, 2007.

24. Ito, T. and J. H. Lunsford, "Synthesis of Ethylene and Ethane by Partial Oxidation of Methane over Lithium-Doped Magnesium Oxide", *Nature*, Vol. 314, No. 6013, pp. 721-722, 1985.

25. Lunsford, J. H., M. D. Cisneros, P. G. Hinson, Y. Tong, and H. Zhang, "Oxidative Dimerization of Methane over Well Defined Lithium-Promoted Magnesium Oxide Catalysts", *Faraday Discussions of the Chemical Society*, Vol. 87, No. 1, pp. 13-21, 1989.

26. Chevalier, C., P. R. de la Piscina, M. Ceruso, A. Choplin, and J. M. Basset, "Oxidative Dimerization of Methane: A Surface Organometallic Approach to Lithium Doped Magnesia or Silica Catalysts", *Catalysis Today*, Vol. 4, No. 3–4, pp. 433-439, 1989.

27. Roos, J. A., S. J. Korf, A. G. Bakker, N. A. De Bruijn, J. G. Van Ommen, and J. R. H. Ross, "The Oxidative Coupling of Methane: Catalyst Requirements and Process Conditions", *Studies in Surface Science and Catalysis*, Vol. 36, No. 1, pp. 427-432, 1988.

28. Hargreaves, J. S. J., G. J. Hutchings, R. W. Joyner, and C. J. Kiely, "Structural Aspects of Magnesium Oxide Catalysts for the Oxidative Coupling of Methane", *Catalysis Today*, Vol. 10, No. 3, pp. 259-266, 1991.

29. Choudhary, V. R., V. H. Rane, and M. Y. Pandit, "Comparison of Alkali Metal Promoted MgO Catalysts for Their Surface Acidity/Basicity and Catalytic Activity/Selectivity in the Oxidative Coupling of Methane", *Journal of Chemical Technology & Biotechnology*, Vol. 68, No. 2, pp. 177-186, 1997.

30. Korf, S. J., J. A. Roos, N. A. de Bruijn, J. G. van Ommen, and J. R. H. Ross, "Oxidative Coupling of Methane over Lithium Doped Magnesium Oxide Catalysts", *Catalysis Today*, Vol. 2, No. 5, pp. 535-545, 1988.

31. Peng, X. D., D. A. Richards, and P. C. Stair, "Surface Composition and Reactivity of Lithium-Doped Magnesium Oxide Catalysts for Oxidative Coupling of Methane", *Journal of Catalysis*, Vol. 121, No. 1, pp. 99-109, 1990.

32. Hutchings, G., M. Scurrell, and J. Woodhouse, "Oxidative Coupling of Methane Using Li/MgO Catalyst: Re-Appraisal of the Optimum Loading of Li", *Catalysis Letters*, Vol. 5, No. 3, pp. 301-308, 1990.

33. Hutchings, G. J., M. S. Scurrell, and J. R. Woodhouse, "The Role of Surface O- in the Selective Oxidation of Methane", *Journal of the Chemical Society, Chemical Communications*, Vol. 18, pp. 1388-1389, 1987.

34. M. Aigler, J. and J. H. Lunsford, "Oxidative Dimerization of Methane over MgO and Li+/MgO Monoliths", *Applied Catalysis*, Vol. 70, No. 1, pp. 29-42, 1991.

35. Yingli, B., Z. Kaiji, J. Yutao, T. Chiwen, and Y. Xiangguong, "Catalytic Oxidative Coupling of Methane over Alkali, Alkaline Earth and Rare Earth Metal Oxides", *Applied Catalysis*, Vol. 39, No. 1, pp. 185-190, 1988.

36. Chen, Q., P. M. Couwenberg, and G. B. Marin, "Effect of Pressure on the Oxidative Coupling of Methane in the Absence of Catalyst", *AIChE Journal*, Vol. 40, No. 3, pp. 521-535, 1994.

37. Ekstrom, A., R. Regtop, and S. Bhargava, "Effect of Pressure on the Oxidative Coupling Reaction of Methane", *Applied Catalysis*, Vol. 62, No. 1, pp. 253-269, 1990.

38. Edwards, J. H., R. J. Tyler, and S. D. White, "Oxidative Coupling of Methane over Lithium-Promoted Magnesium Oxide Catalysts in Fixed-Bed and Fluidized-Bed Reactors", *Energy & Fuels*, Vol. 4, No. 1, pp. 85-93, 1990.

39. Phillips, M. D. and A. Eastman, "Effect of Li/MgO Methane Coupling Catalyst on Alonized Steel Reactors", *Catalysis Letters*, Vol. 13, No. 3, pp. 157-174, 1992.

40. Chen, Q., P. M. Couwenberg, and G. B. Marin, "The Oxidative Coupling of Methane with Cofeeding of Ethane", *Catalysis Today*, Vol. 21, No. 2–3, pp. 309-319, 1994.

41. Taniewski, M., A. Lachowicz, K. Skutil, and D. Czechowicz, "The Effect of Dilution of the Catalyst Bed on Its Heat-Transfer Characteristics in Oxidative Coupling of Methane", *Chemical Engineering Science*, Vol. 51, No. 18, pp. 4271-4278, 1996.

42. Kiatkittipong, W., T. Tagawa, S. Goto, S. Assabumrungrat, K. Silpasup, and P. Praserthdam, "Comparative Study of Oxidative Coupling of Methane Modeling in Various Types of Reactor", *Chemical Engineering Journal*, Vol. 115, No. 1–2, pp. 63-71, 2005.

43. Olivier, L., S. Haag, C. Mirodatos, and A. C. van Veen, "Oxidative Coupling of Methane Using Catalyst Modified Dense Perovskite Membrane Reactors", *Catalysis Today*, Vol. 142, No. 1–2, pp. 34-41, 2009.

44. Roussy, G., E. Marchal, J. M. Thiebaut, A. Kiennemann, and G. Maire, "C_{2+} Selectivity Enhancement in Oxidative Coupling of Methane over Microwave-Irradiated Catalysts", *Fuel Processing Technology*, Vol. 50, No. 2–3, pp. 261-274, 1997.

45. Roos, J. A., S. J. Korf, J. J. P. Biermann, J. G. van Ommen, and J. R. H. Ross, "Oxidative Coupling of Methane, the Effect of Gas Composition and Process Conditions", *Studies in Surface Science and Catalysis*, Vol. 55, No. 1, pp. 381-392, 1990.

46. Korf, S. J., J. A. Roos, L. J. Veltman, J. G. van Ommen, and J. R. H. Ross, "Effect of Additives on Lithium Doped Magnesium Oxide Catalysts Used in the Oxidative Coupling of Methane", *Applied Catalysis*, Vol. 56, No. 1, pp. 119-135, 1989.

47. Larkins, F. P. and M. R. Nordin, "The Effects of Transition Metal Oxides on the Methane Oxidative Coupling Activity of Doped MgO Catalysts I. Zinc and Manganese", *Journal of Catalysis*, Vol. 130, No. 1, pp. 147-160, 1991.

48. Hoogendam, G. C., K. Seshan, J. G. van Ommen, and J. R. H. Ross, "Oxidative Coupling of Methane over Doped Li/MgO Catalysts", *Catalysis Today*, Vol. 21, No. 2–3, pp. 333-340, 1994.

49. McNamara, D. J., S. J. Korf, K. Seshan, J. G. Van Ommen, and J. R. H. Ross, "The Effect of Nb_2O_5 and ZrO_2 Additions on the Behaviour of Li/MgO and Li/Na/MgO Catalysts for the Oxidative Coupling of Methane", *The Canadian Journal of Chemical Engineering*, Vol. 69, No. 4, pp. 883-890, 1991.

50. Tiwari, K. K., T. N. Roy, S. Banerjee, S. Ganguly, and D. P. Bhattacharyya, "Oxidative Coupling of Methane to C_2-Hydrocarbons over Lithium–Cerium-Promoted MgO and MgO–Cao Catalysts", *Journal of Chemical Technology & Biotechnology*, Vol. 63, No. 2, pp. 190-194, 1995.

51. Lunsford, J. H., P. G. Hinson, M. P. Rosynek, C. L. Shi, M. T. Xu, and X. M. Yang, "The Effect of Chloride Ions on a Li+-MgO Catalyst for the Oxidative Coupling of Methane", *Journal of Catalysis*, Vol. 147, No. 1, pp. 301-310, 1994.

52. Abraham, M. M., Y. Chen, L. A. Boatner, and R. W. Reynolds, "Stable $[Li]^0$ Defects in MgO Single Crystals", *Physical Review Letters*, Vol. 37, No. 13, pp. 849-852, 1976.

53. Driscoll, D. J., W. Martir, J. X. Wang, and J. H. Lunsford, "Formation of Gas-Phase Methyl Radicals over Magnesium Oxide", *Journal of the American Chemical Society*, Vol. 107, No. 1, pp. 58-63, 1985.

54. Sokolovskii, V. D., S. M. Aliev, O. V. Buyevskaya, and A. A. Davydov, "Type of Hydrocarbon Activation and Nature of Active Sites of Base Catalysts in Methane Oxidative Dehydrodimerization", *Catalysis Today*, Vol. 4, No. 3–4, pp. 293-300, 1989.

55. Passos, F. B., M. Schmal, and M. A. Vannice, "Effect of in and Sn on the Adsorption Behavior and Hydrogenolysis Activity of Pt/Al_2O_3catalysts", *Journal of Catalysis*, Vol. 160, No. 1, pp. 106-117, 1996.

56. van Kasteren, J. M. N., J. W. M. H. Geerts, and K. v. der Wiele, "Methane Oxidative Coupling Using Li/MgO Catalysts: The Importance of Consecutive Reactions", *Studies in Surface Science and Catalysis*, Vol. 61, No. 1, pp. 139-146, 1991.

57. Spencer, M. S., J. H. Lunsford, M. W. Roberts, J. Cunningham, R. Burch, O. V. Krylov, J. B. Moffat, G. J. Hutchings, R. W. Joyner, M. Ichikawa, A. K. Datye, J. Haber, E. M. Serwicka, and J. M. Thomas, "General Discussion", *Faraday Discussions of the Chemical Society*, Vol. 87, No. 1, pp. 47-64, 1989.

58. Mirodatos, C., V. Perrichon, M. C. Durupty, and P. Moral, "Deactivation of Alkali Promoted Magnesia in Oxidative Coupling of Methane", *Studies in Surface Science and Catalysis*, Vol. 34, No. 1, pp. 183-195, 1987.

59. Hammond, C., S. Conrad, and I. Hermans, "Oxidative Methane Upgrading", *ChemSusChem*, Vol. 5, No. 9, pp. 1668-1686, 2012.

60. Tomašić, V. and F. Jović, "State-of-the-Art in the Monolithic Catalysts/Reactors", *Applied Catalysis A: General*, Vol. 311, No. 1, pp. 112-121, 2006.

61. Nijhuis, T. A., A. E. W. Beers, T. Vergunst, I. Hoek, F. Kapteijn, and J. A. Moulijn, "Preparation of Monolithic Catalysts", *Catalysis Reviews*, Vol. 43, No. 4, pp. 345-380, 2001.

62. Campanati, M., G. Fornasari, and A. Vaccari, "Fundamentals in the Preparation of Heterogeneous Catalysts", *Catalysis Today*, Vol. 77, No. 4, pp. 299-314, 2003.

63. Vergunst, T., F. Kapteijn, and J. A. Moulijn, "Monolithic Catalysts — Non-Uniform Active Phase Distribution by Impregnation", *Applied Catalysis A: General*, Vol. 213, No. 2, pp. 179-187, 2001.

64. Pérez-Cadenas, A. F., M. M. P. Zieverink, F. Kapteijn, and J. A. Moulijn, "High Performance Monolithic Catalysts for Hydrogenation Reactions", *Catalysis Today*, Vol. 105, No. 3–4, pp. 623-628, 2005.

65. Andersen, A. G. and T. Norby, "Liquid Phases in Li:MgO as Studied by Thermoanalytical Methods, Electron Microscopy, and Electrical Conductivity Measurements", *Catalysis Today*, Vol. 6, No. 4, pp. 575-586, 1990.

66. Düşova, Y., *An Experimental Study on Oxidative Coupling of Methane over $Mn/Na_2WO_4/SiO_2$ Catalyst*, M.S. Thesis, Boğaziçi University, 2014.

67. Sezen, S., *Oxidative Coupling of Methane over Lanthanum and Strontium Promoted Magnesium Catalyst,* M.S. Thesis, Boğaziçi University, 2014.

68. Zhang, Y., M. K. Ram, E. K. Stefanakos, and D. Y. Goswami, "Synthesis, Characterization, and Applications of Zno Nanowires", *Journal of Nanomaterials*, Vol. 2012, No. 1, pp. 1-22, 2012.

69. Sugunan, A., V. K. Guduru, A. Uheida, M. S. Toprak, and M. Muhammed, "Radially Oriented Zno Nanowires on Flexible Poly-L-Lactide Nanofibers for Continuous-Flow Photocatalytic Water Purification", *Journal of the American Ceramic Society*, Vol. 93, No. 11, pp. 3740-3744, 2010.

70. Zhong Lin, W., "Zinc Oxide Nanostructures: Growth, Properties and Applications", *Journal of Physics: Condensed Matter*, Vol. 16, No. 25, pp. R829, 2004.

71. Hong, X. and Y. Wang, "Partial Oxidation of Methane to Syngas Catalyzed by a Nickel Nanowire Catalyst", *Journal of Natural Gas Chemistry*, Vol. 18, No. 1, pp. 98-103, 2009.

72. Flame Spray Technology Co., "Principles of Thermal Spraying", 2009, http://www.fst.nl/principles-of-thermal-spraying, [Accessed Jun 2015].

73. Rudnev, V., Taylor, and Francis, *Handbook of Induction Heating*. Vol. 61., New York: Marcel Dekker, 2003.